UNCLASSIFIED

AD 267 163

Reproduced
by the

ARMED SERVICES TECHNICAL INFORMATION AGENCY
ARLINGTON HALL STATION
ARLINGTON 12, VIRGINIA

UNCLASSIFIED

AFCRL 940

Final Report

STUDY OF THE EFFECTS OF ENVIRONMENTAL CONDITIONS ON THE BREAKDOWN OF ANTENNAS AT LOW PRESSURES ON A SUPERSONIC VEHICLE

Prepared for

ELECTRONICS RESEARCH DIRECTORATE
AIR FORCE CAMBRIDGE RESEARCH LABORATORIES
OFFICE OF AEROSPACE RESEARCH
UNITED STATES AIR FORCE
BEDFORD, MASSACHUSETTS

CONTRACT AF 19(604)-5483

By: J. B. Chown M. G. Keenan

STANFORD RESEARCH INSTITUTE
MENLO PARK, CALIFORNIA

SRI

Requests for additional copies by Agencies of the Department of Defense, their contractors, and other Government agencies should be directed to the:

ARMED SERVICES TECHNICAL INFORMATION AGENCY
ARLINGTON HALL STATION
ARLINGTON 12, VIRGINIA

Department of Defense contractors must be established for ASTIA services or have their "need-to-know" certified by the cognizant military agency of their project or contract.

All other persons and organizations should apply to the:

U.S. DEPARTMENT OF COMMERCE
OFFICE OF TECHNICAL SERVICES
WASHINGTON 25, D.C.

STANFORD RESEARCH INSTITUTE
MENLO PARK, CALIFORNIA

September 1961

AFCRL 940

Final Report

STUDY OF THE EFFECTS OF ENVIRONMENTAL CONDITIONS ON THE BREAKDOWN OF ANTENNAS AT LOW PRESSURES ON A SUPERSONIC VEHICLE

Prepared for:

ELECTRONICS RESEARCH DIRECTORATE
AIR FORCE CAMBRIDGE RESEARCH LABORATORIES
OFFICE OF AEROSPACE RESEARCH
UNITED STATES AIR FORCE
BEDFORD, MASSACHUSETTS

CONTRACT AF 19(604)-5483

By: *J. B. Chown* *M. G. Keenan*

SRI Project No. 2879

Approved:

D. R. SCHEUCH, DIRECTOR - ELECTRONICS AND RADIO SCIENCES DIVISION

Copy No. 111

ABSTRACT

The breakdown characteristics of antennas under supersonic flight conditions at altitudes up to 80 miles were investigated. Three Nike-Cajun rockets were instrumented and fired from Eglin Gulf Test Range on 4 November 1960 and on 14 and 24 March 1961. Significant results were obtained only from the 14 March firing.

Details of the instrumentation are given, as well as a discussion of the data obtained. Data are given on the RF power required to initiate and extinguish breakdown, surface temperatures, and pressure on the surface of the conical nose. A comparison of breakdown data with previously obtained laboratory data and with the theory of breakdown phenomena reveals discrepancies which remain unresolved due to the limited quantity of flight data available for analysis.

CONTENTS

CONTENTS

ILLUSTRATIONS

TABLES

I INTRODUCTION

Telemetry and tracking signals from rockets and missiles have frequently been subjected to severe degradation caused by RF breakdown of the vehicle antenna. Previous experimental studies to evaluate the effects of this breakdown phenomenon have mainly been conducted in the laboratory, in which static pressure and room temperature conditions prevailed. The primary goal of the investigation reported herein was to study the breakdown characteristics of antennas subjected to the dynamic conditions encountered in supersonic flight. The information thus obtained would provide a means of determining the ability of the laboratory vacuum-chamber data to predict the performance of antennas on hypersonic vehicles.

The breakdown of antennas at low pressure has been studied in the past by various investigators[1-3]* and it has been shown that the primary source of ionization is electron motion. The equation which describes this mechanism is

$$\frac{\partial n}{\partial t} = (\nu_i - \nu_a) n + \nabla^2 (Dn) + S \qquad (1)$$

where n is the electron density, ν_i is the frequency of ionization per electron, ν_a is the frequency of attachment per electron, D is the diffusion coefficient, and S is the rate of production of electrons by an external source. For breakdown to occur, the rate of change of electron density with time ($\partial n/\partial t$) must be slightly greater than zero. Under these conditions the electron density will increase exponentially with time at a rate determined by $\partial n/\partial t$, which is the value of the difference between electron production and loss rates.

For the pulse breakdown case Eq. (1) can be integrated over a time period of the pulse, τ, to obtain the final density, n. Performing the integration and making the substitution that $\nabla^2(Dn)/n = -D/\Lambda^2$, which is obtained from steady state solutions of Eq. (1).

* References are listed at the end of the report.

$$\frac{\nu_i}{p} = \frac{\nu_a}{p} + \frac{Dp}{(p\Lambda)^2} + \frac{ln\frac{n_\tau}{n_0}}{p\tau} \quad . \tag{2}$$

Here Λ has the dimensions of length and is a characteristic diffusion length for the particular geometry and conditions being considered. The pressure term included in Eq. (2) is necessary to account for the effects of density changes on the various rates.[4] The initial source term, S, is eliminated except that it established the initial value of electron density n_0.

ν_i in Eq. (2) is taken as the value of electron production rate per electron required to produce breakdown, while the quantities on the right side of Eq. (2) constitute the loss rates by attachment, diffusion and the additional increment of ν_i required for breakdown during the pulse length τ. The value of n_τ is assumed to be approximately equal to the electron density associated with the plasma frequency, $f_p = 9 \times 10^3 n^{1/2}$, where f_p is the frequency of the applied electric field.

In order to determine the electric field required to produce breakdown the relationship between ν_i and E_e must be known. E_e is the effective field which would produce the same energy transfer to the electrons as a dc field and is given by

$$E_e = \frac{E\nu_c}{(\nu_c^2 + \omega^2)^{1/2}} \tag{3}$$

where E is the rms field, ω is the angular frequency of the applied field and ν_c is the collision frequency.

The equation describing breakdown under CW conditions is the same as Eq. (2) with the exception that, for CW, $\tau \to \infty$ and $(ln\ n_\tau/n_0)/p\tau \to 0$. Thus Eq. (2) becomes

$$\frac{\nu_i}{p} = \frac{\nu_a}{p} + \frac{Dp}{(p\Lambda)^2} \quad . \tag{4}$$

The principal means by which antenna breakdown is changed by the dynamic conditions of supersonic flight below about $M = 6$, which is the speed regime of interest here, is through the modification of the gas density and temperature adjacent to the antenna due to aerodynamic effects. Examination of the equations describing pulse and CW breakdown indicate the dependence of the electron production rate, ν_i, as well as all the loss mechanisms (attachment, diffusion, and time-dependent term) on density. The relation between E_c and E_{rms}, Eq. (3), which is dependent on the collision frequency, and thus density and temperature, is also modified by flight conditions and must be considered.

In missile systems where very high velocities are encountered, $M > 10$, ionization due to aerodynamic heating and velocity effects may become sufficient to further modify the required breakdown field.

Since breakdown results are somewhat different for pulsed and CW radiations, tests were performed for each of these conditions. After power output, size and weight, and complexity of available equipment were considered, it was decided to perform the pulse experiment in the X-band frequency range and the CW experiment in the VHF range. Laboratory tests and theory indicate that for a given frequency, antenna configuration, and maximum power, breakdown can be expected to take place over a certain range of gas densities. In the atmosphere the air density is a function of altitude. Figure 1 shows the approximate altitude regions at which breakdown would be expected for VHF and X-band narrow slot antennas where the power available is 30 watts CW and 7.0 kw peak, respectively. Also shown are velocity and altitude characteristics of a typical Nike-Cajun research rocket with an 80-lb payload. It can be seen that this rocket has the altitude capabilities required, as well as supersonic speed capability throughout the breakdown altitude regions. Because of these essential characteristics and because of its relative cheapness and ease of firing, the Nike-Cajun rocket combination was chosen as the vehicle for the test instrumentation.

A second goal, which was introduced later in the program, was to investigate the buildup of charge on the surface of the rocket during flight.

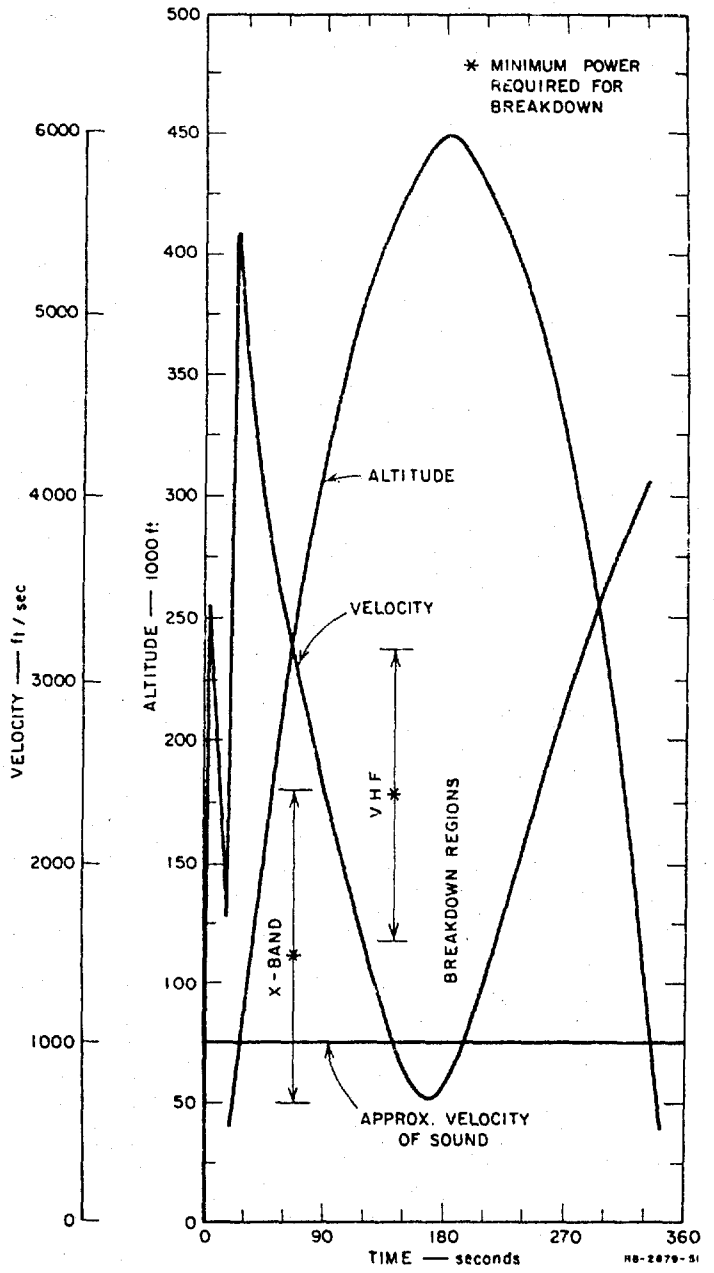

FIG. 1 TYPICAL NIKE-CAJUN VELOCITY AND ALTITUDE CHARACTERISTICS

Finally, a third goal was to investigate the effects of the ionosphere on very-low-frequency (VLF) signals. This investigation was part of another contract* which was sponsored by U.S. Navy, Bureau of Naval Weapons Special Projects Office and conducted by SRI personnel on a non-interference basis. The results of that investigation have been reported separately.[5]

* Contract NOw-60-0405(FBM)

II INSTRUMENTATION

A. GENERAL

Three rocket instrumentation packages assembled by SRI were fired[6] from Eglin Gulf Test Range, Eglin Air Force Base, Florida, in November of 1960 and March of 1961. The instrumentation consisted of an *X*-band transmitter and antenna; a VHF transmitter and antenna; *X*-band and VHF detectors; a telemetry system; common power supply; and pressure and temperature sensors. In addition to these equipments there were a VLF receiver, magnetometer and a field strength meter which were used to carry out the VLF-propagation and missile-charging experiments mentioned in Sec. II. The VHF and *X*-band transmitters and the common power supply were built on a sub-contract with Granger Associates. The remainder of the equipment was either built or purchased and installed by the Institute. Standard systems and components were used wherever possible to reduce cost and complexity.

Figure 2 shows the basic arrangement of antennas and temperature and pressure sensors. Figure 3 shows the space allocations for all major equipments. Figure 4 is a photograph of one of the completed packages with cover removed. Figure 5 shows the nose cone section. The design goal for total weight was approximately 60 lbs. However, the addition of two experiments raised the final total weight of the equipment package to 80 lbs.

Several methods of data collection were employed. The RF pulses radiated by the *X*-band antenna were detected by ground receiving equipment, and the resulting video outputs were displayed on an oscilloscope screen and photographed. The CW signals radiated by the VHF antenna were detected by ground receiving equipment which recorded the AGC voltage. The rocket velocity, acceleration, and position data were obtained from tracking radars and Contraves phototheodolites. A beacon was carried on each flight to assure good tracking by the radars. The remainder of the data were telemetered and recorded using standard FM/FM telemetry equipment.

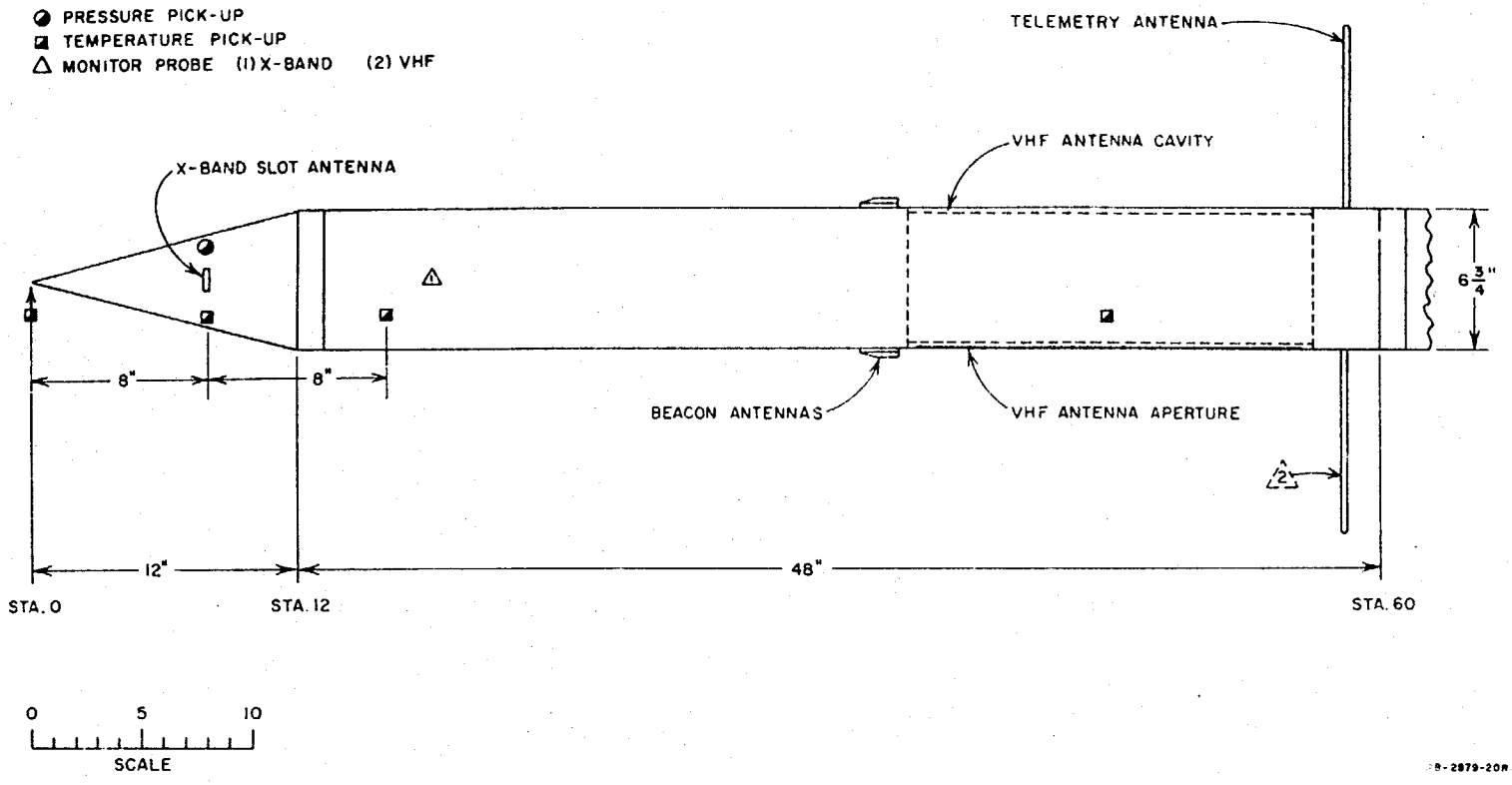

FIG. 2 BASIC CONFIGURATION OF ANTENNAS AND ENVIRONMENT SENSORS

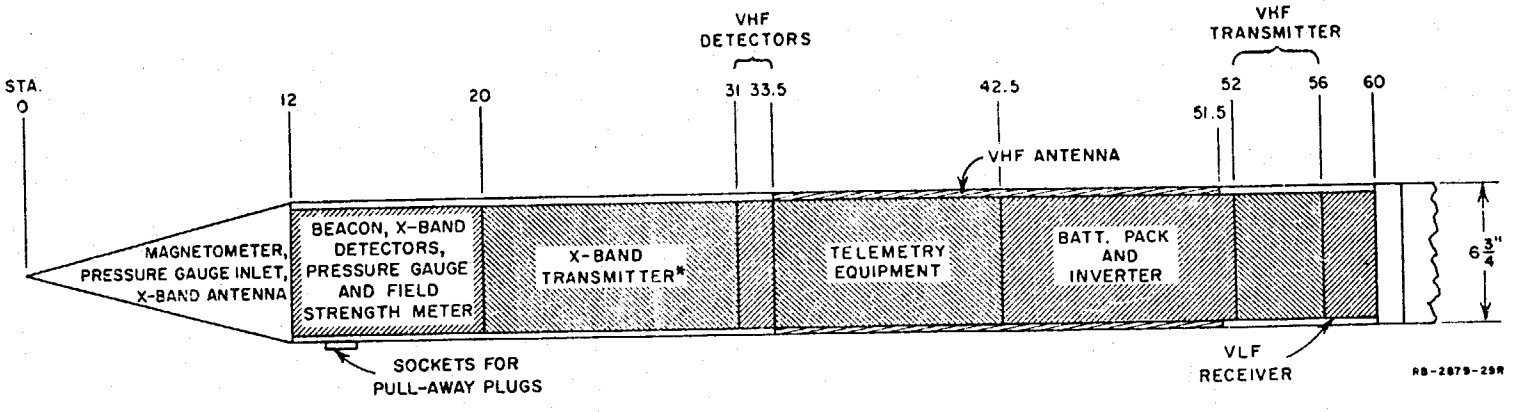

FIG. 3 ARRANGEMENT OF EQUIPMENT IN INSTRUMENTATION PACKAGE

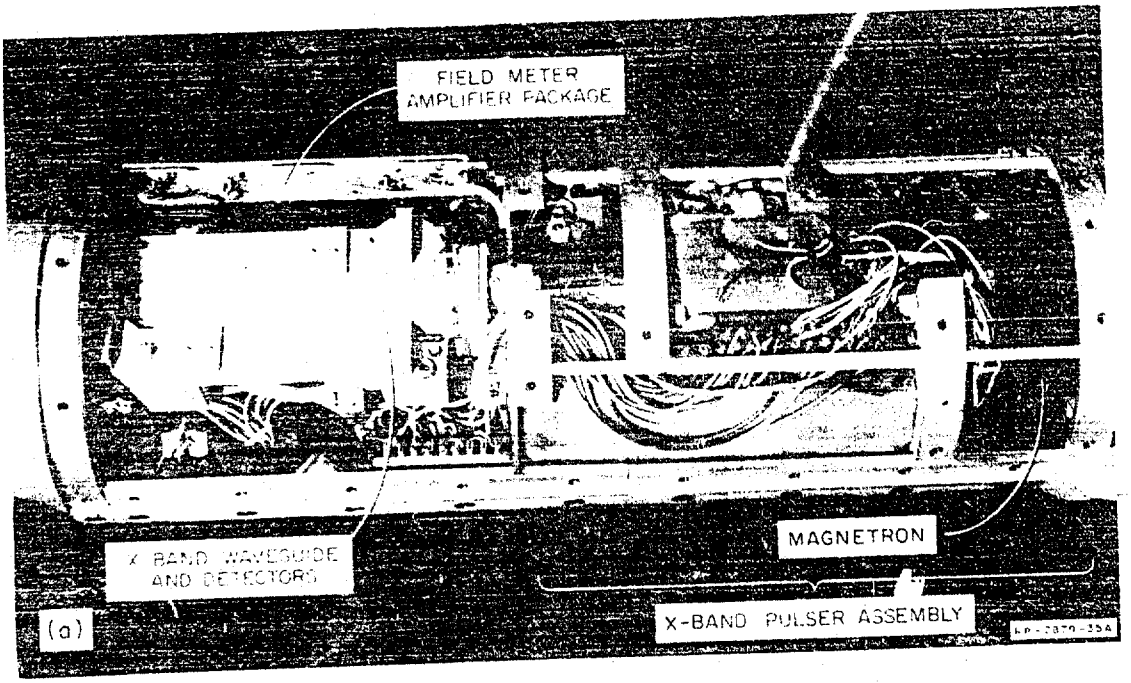

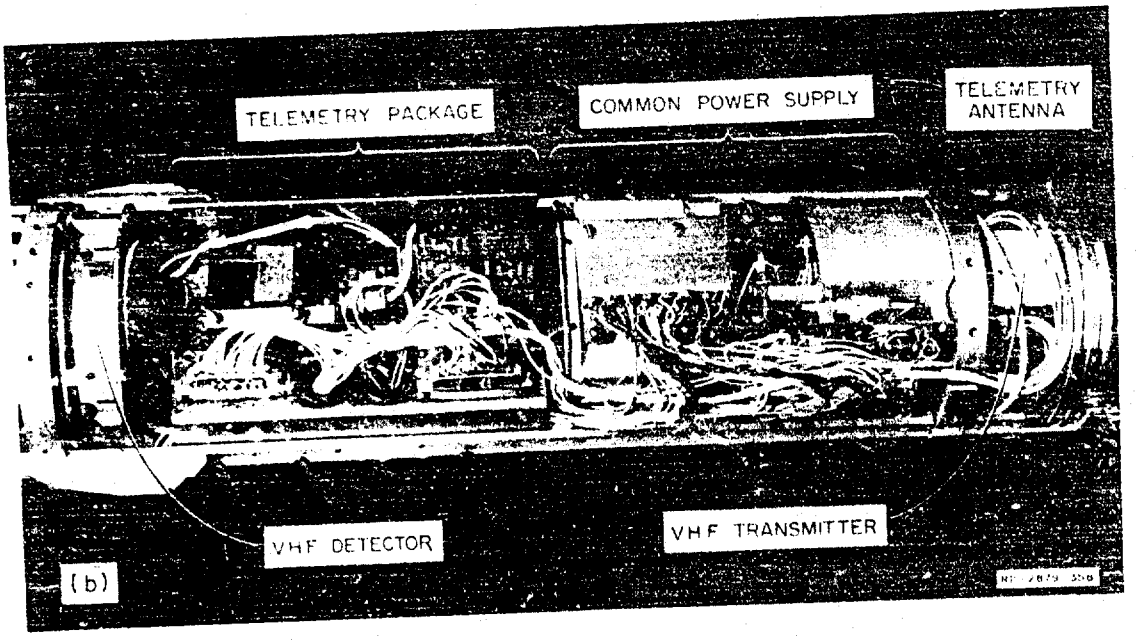

FIG. 4 COMPLETED INSTRUMENTATION PACKAGE WITH COVER REMOVED

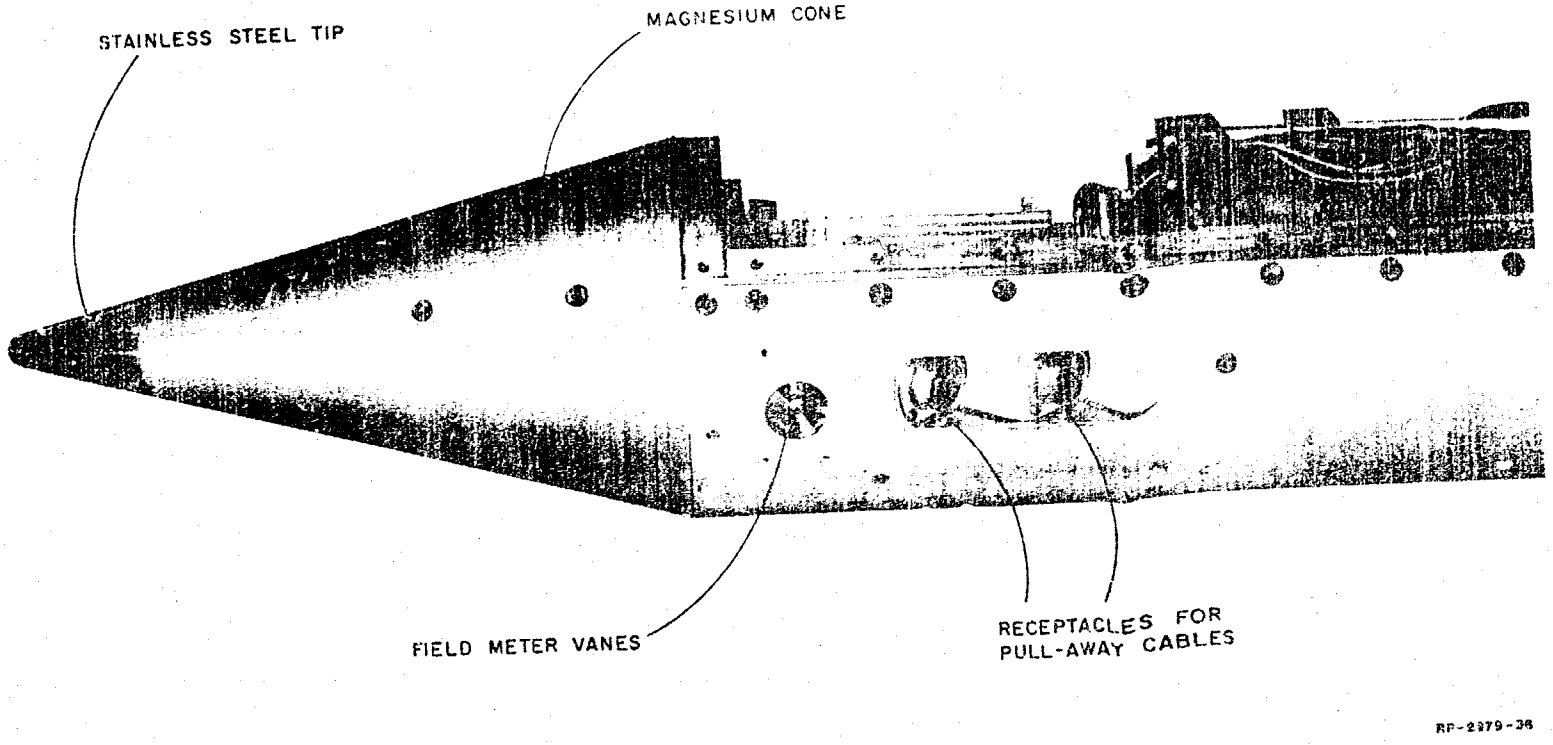

FIG. 5 NOSECONE SECTION

B. ANTENNA BREAKDOWN

1. VHF

The VHF system consisted of a CW transmitter, detectors, a narrow-slot test antenna, a short-stub sampling antenna (for sampling power transmitted by the test antenna), and a dual coaxial-line coupler (see Fig. 6).

The transmitter consisted of a driver and two power amplifiers and was amplitude-modulated approximately linearly so that the power output varied from a maximum of 30 watts (nominal) to a minimum of 1 watt (nominal). This was done to initiate and extinguish the antenna breakdown repeatedly throughout the flight. It is known that when breakdown occurs the amounts of power reflected and transmitted change suddenly, and the resulting step in the observed modulation envelopes can be used to indicate the point in the modulation cycle at which the breakdown occurs. This, together with a knowledge of the slope of the power modulation envelope, enables an accurate determination of the power level at which breakdown is initiated. The extinguish level can be determined in the same manner. This technique was used in this study. A one-cycle-per-second modulation rate was chosen because it was rapid enough to complete one cycle of the power swing with a relatively small change in vehicle altitude and yet slow enough to permit adequate telemetry sampling of the modulation wave.

The detectors were d-c self-compensating Wheatstone bridges with resistance arms (see Fig. 7a). Two arms were fixed precision resistors; the active, or "unknown" arm was an N-610B bolometer which was also coupled to the RF circuit; the fourth arm was a N-610B bolometer which was not coupled to the RF circuit. This latter bolometer was used to compensate for unbalances resulting from temperature changes in the active bolometer. Potentiometer R7 was used to make the slope of the resistance-temperature curve of the compensating bolometer equal to that of the active bolometer. The RF circuit was coupled to the active bolometer through a high-pass filter with cutoff slightly above 234 Mc to prevent coupling of the telemetry signals to the bridge detector. The isolation achieved between the VHF frequency of 259.7 Mc and the telemetry frequency of 234 Mc was greater than 20 db. Potentiometer R8 was used

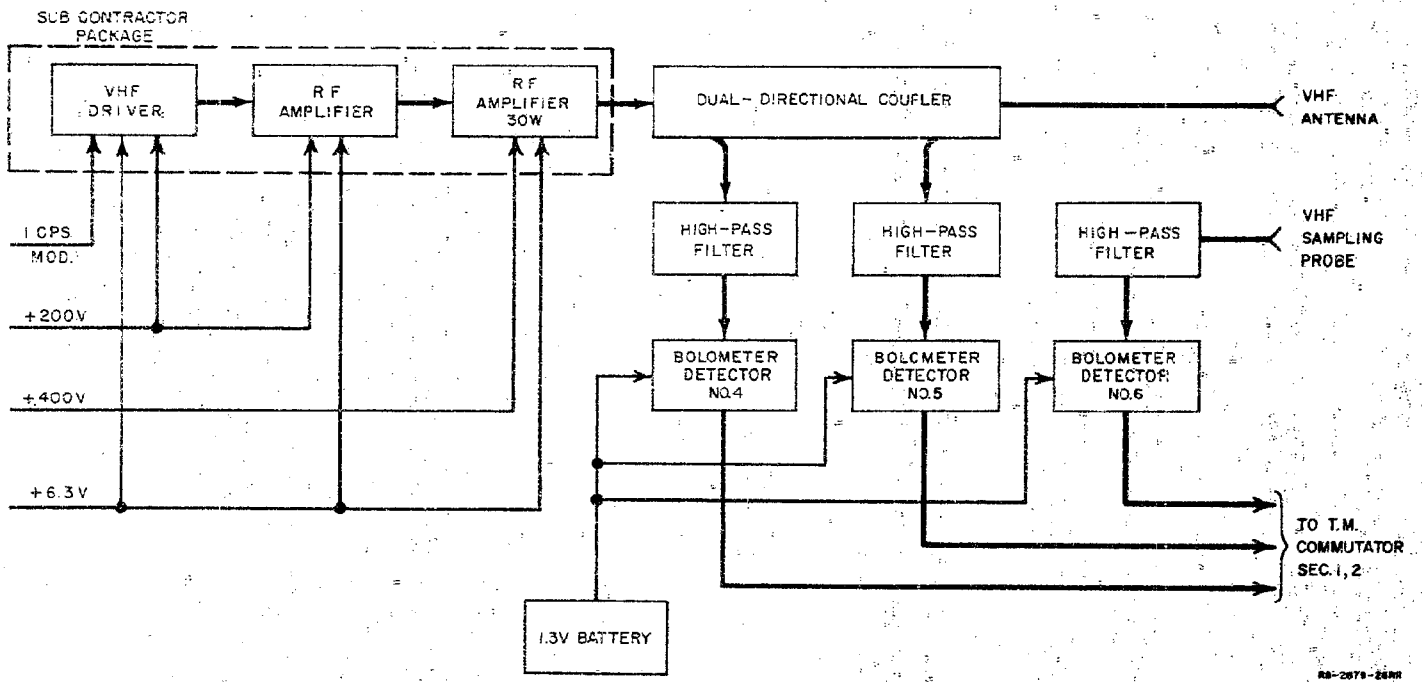

FIG. 6 BLOCK DIAGRAM OF VHF TRANSMITTER

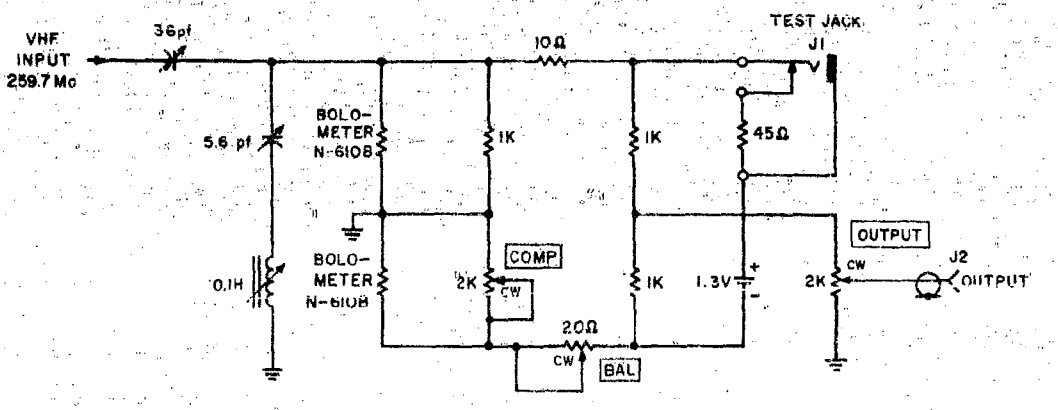

(a) VHF DETECTOR

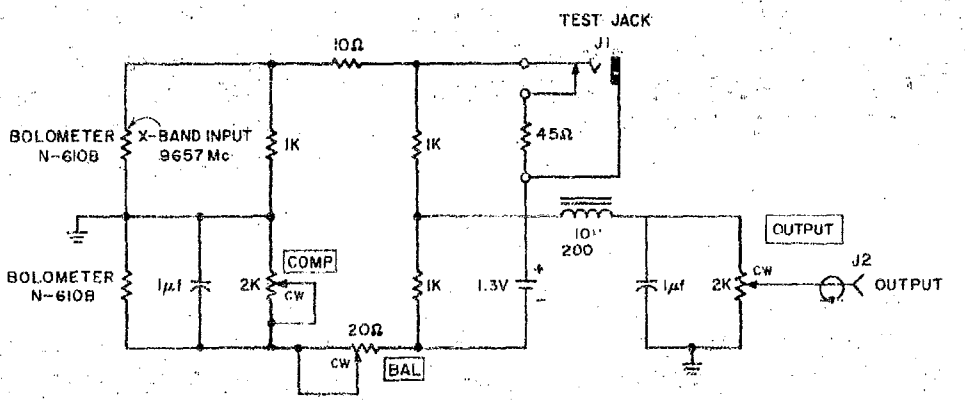

(b) X-BAND DETECTOR

8-2879-37

FIG. 7 SCHEMATIC DIAGRAM OF BOLOMETER BRIDGE CIRCUIT

to set the initial bridge balance, and R11 was used to adjust the output level. Typical over-all sensitivity was 2.0 mv output per mw of average RF power input (see Fig. 8).

Three such detectors were employed to measure the amounts of power incident on, reflected from, and transmitted by the slot test antenna. These bridges were potted and mounted adjacent to each other on a common base which was removable from the rocket for tuning and for battery replacement (see Fig. 9). A coaxial dual coupler was located between the transmitter and antenna to permit sampling the incident and reflected power. This coupler had a coupling factor of 30 db and a

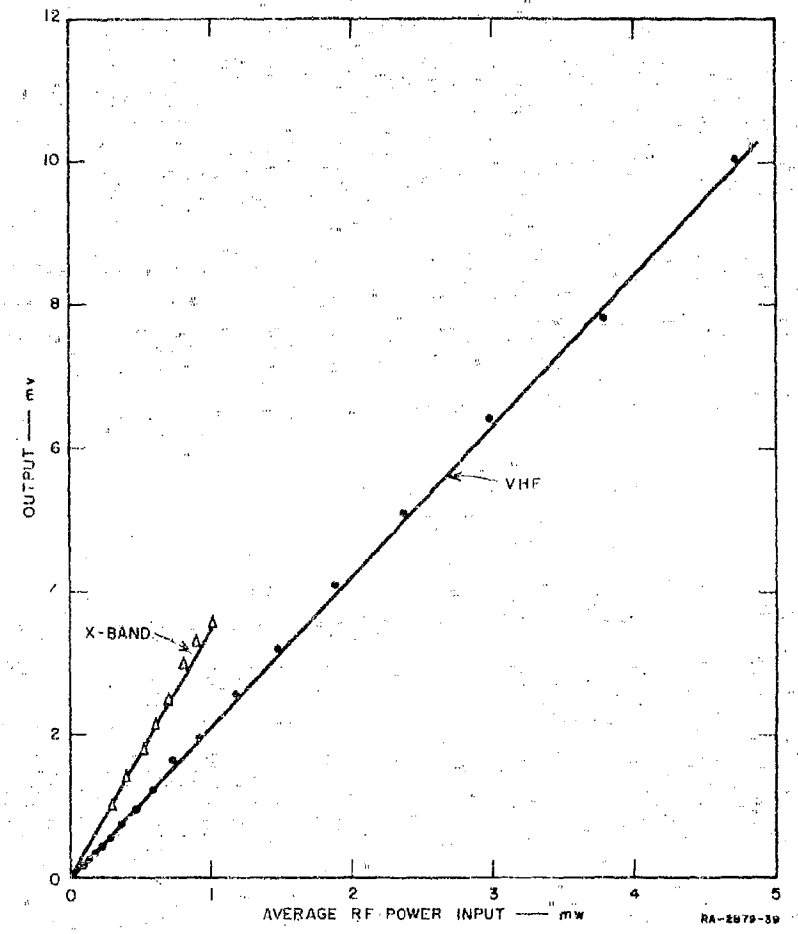

FIG. 8 RESPONSE CURVE FOR BOLOMETER BRIDGE CIRCUIT

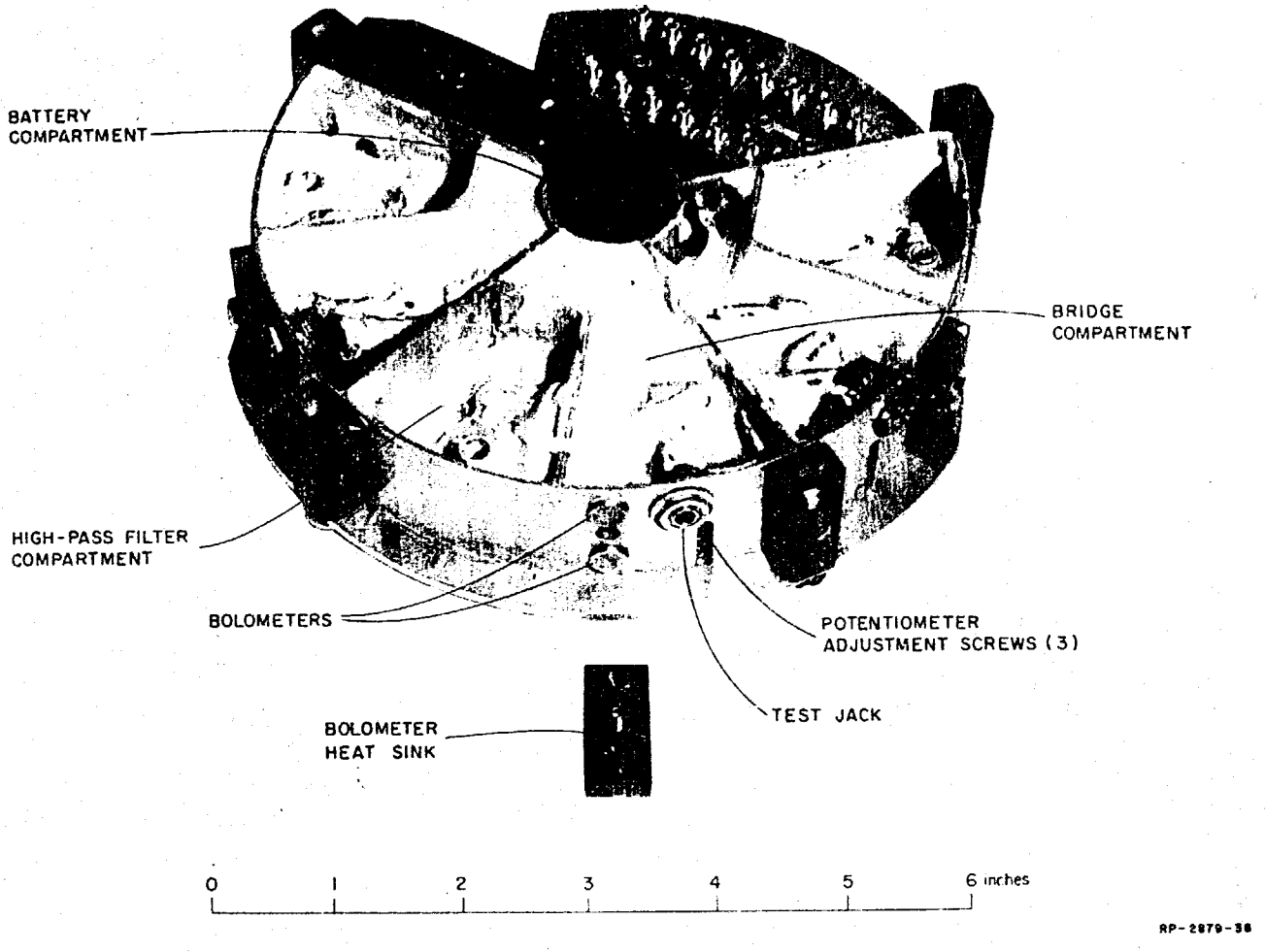

FIG. 9 COMPLETED VHF DETECTOR ASSEMBLY WITH COVER REMOVED

directivity of 30 db. A stub antenna was used as a probe for sampling the transmitted power (see Fig. 2). Decoupling between the stub and the test antenna was found to be about 40 db; therefore no further decoupling was required and the sampling stub was connected directly to the input of one of the bridge detectors.

The test antenna was a cavity-backed narrow slot antenna, with the rocket skin acting as the ground plane (see Fig. 10). The $\frac{1}{8}$-inch aperture was narrow enough to break down in the altitude region of 120,000 to 240,000 ft. The use of a conventional straight-section backing cavity was not possible due to the small rocket diameter in terms of the wavelength. Instead, a wrap-around type of cavity was used, as shown in Fig. 10. This was equivalent to a waveguide feed with a very small b dimension ($\frac{1}{4}$-inch) and low characteristic impedance. In addition, the a dimension (18-inches) was too small to permit propagation, if air were used as the dielectric. A dielectric material with a dielectric constant greater than 2 was required. Originally a material with a dielectric constant of 2.5 and a loss tangent of 0.013 was used. This consisted of a resin in honeycomb form, which provided great mechanical strength. The resulting antenna was carefully tuned at the operating frequency of 259.7 Mc by adjusting the location and size of the feed probe. The maximum VSWR after tuning was 1.5 over the band from 259 Mc to 261 Mc. However, the insertion loss was measured and found to be greater than

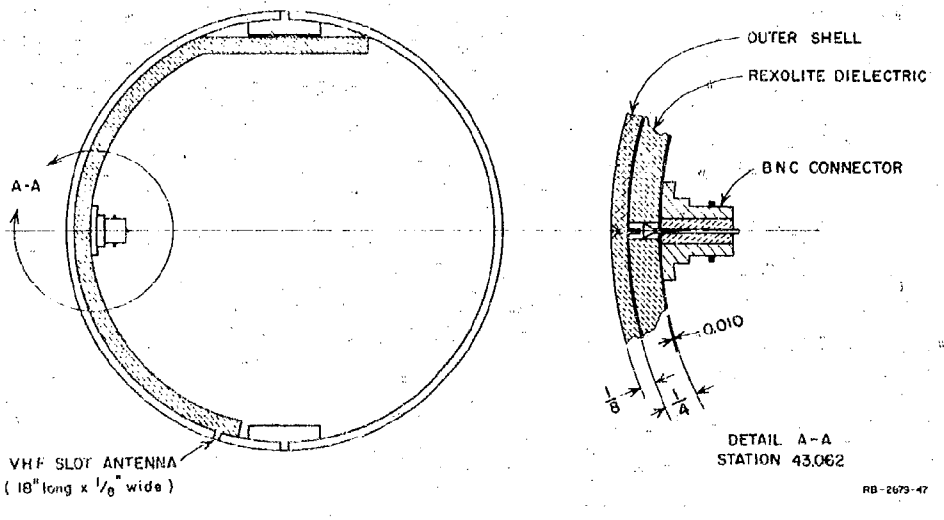

FIG. 10 VHF ANTENNA DETAILS

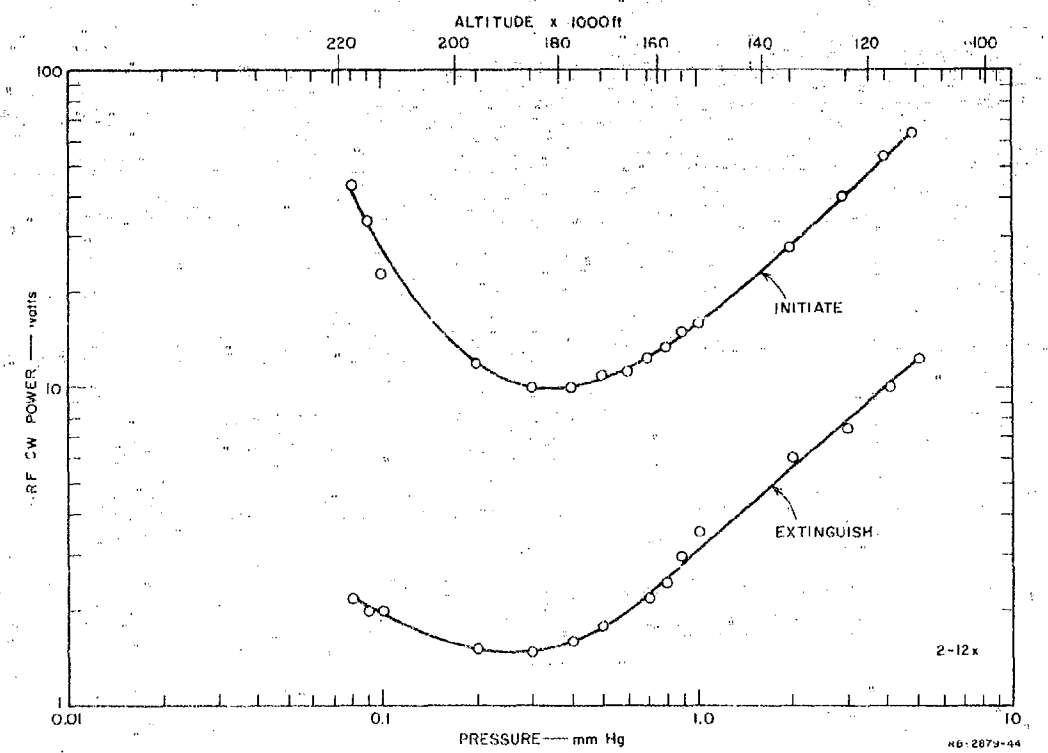

FIG. 11 VHF ANTENNA BREAKDOWN RESULTS – LABORATORY TEST

7 db, which is considered excessive in view of the fact that most of the power delivered by the transmitter is required to assure a high enough field at the slot to cause breakdown. A second prototype was constructed with Rexolite as the dielectric. This material has a dielectric constant of 2.8 and a loss tangent of 0.0006. After being matched to the same specifications as before, this antenna was found to have an insertion loss of only 4 db. Breakdown tests were performed on the flight-model antennas in the laboratory vacuum chamber. The results of the test on the antenna used in the 14 March firing are given in Fig. 11.

2. *X*-Band

The *X*-band system, which was similar to the VHF system, is shown in Fig. 12. The basic differences were the use of pulsed, rather than CW energy, and the use of waveguide transmission line instead of coaxial cables.

A pulsed magnetron with a frequency of 9,657 Mc and a maximum peak output of 7 kw was used as the power source. The pulsed output power

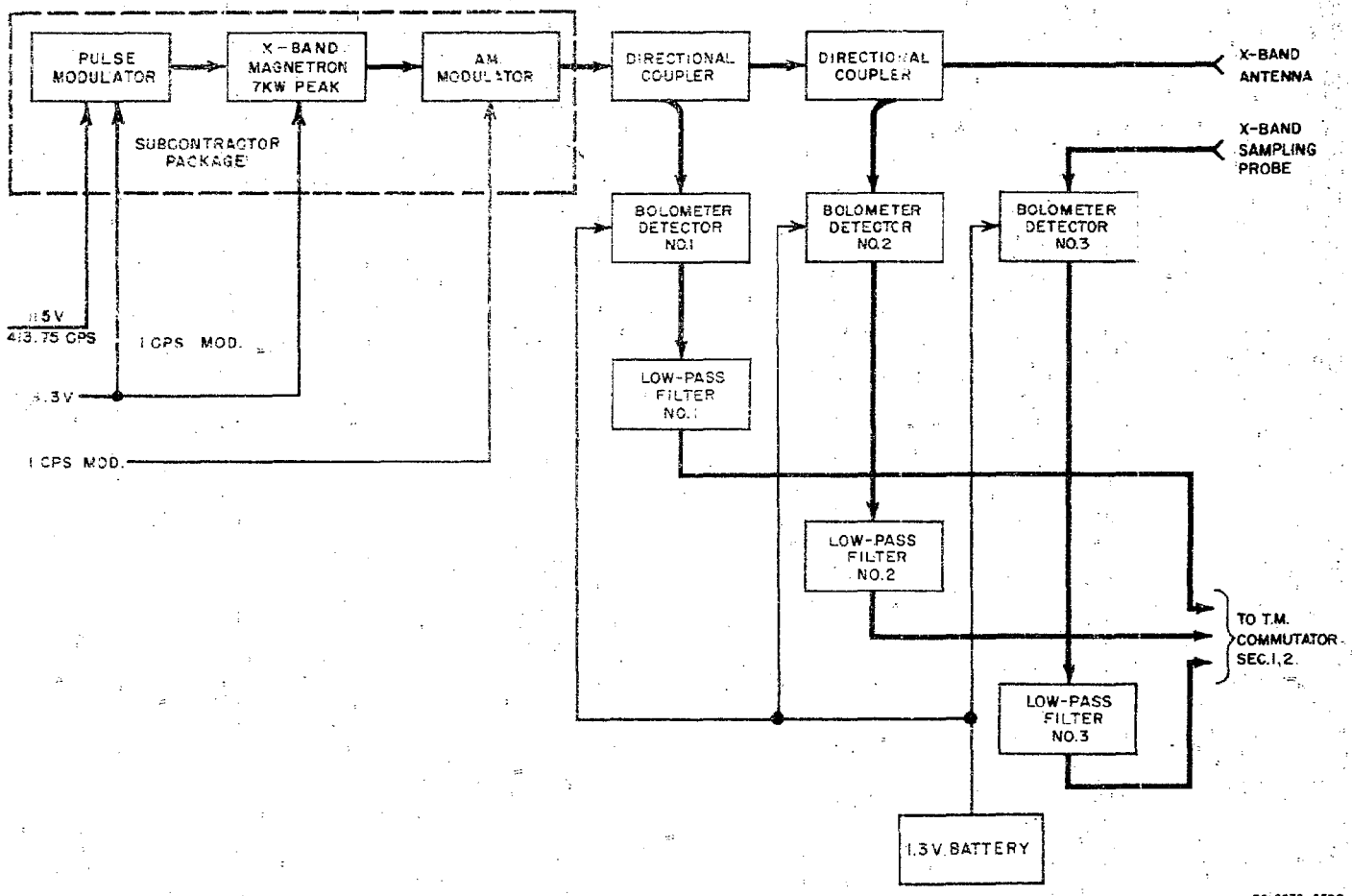

FIG. 12 BLOCK DIAGRAM OF X-BAND TRANSMITTER

of this transmitter was slowly varied by applying 1-cps modulation voltage to a ferrite modulator in the RF line. The peak power output thus increased and decreased approximately linearly, with a maximum of 7 kw and a minimum of 700 watts.

The detectors were basically the same as the VHF detectors described, except that the waveguide itself was used as the input high-pass filter and a low-pass output filter was added to obtain a slowly-varying output from the video pulses. Also, a 1-μf capacitor was connected across the compensating bolometer to bypass the video pulses which feed back through the battery (see Fig. 7b). Typical over-all sensitivity was 3.5 mw output per mw of average RF power input (see Fig. 8).

Three bridge detectors were employed in the *X*-band system to measure incident, reflected, and transmitted power. Two of these detectors were integral parts of a waveguide dual coupler inserted between the transmitter and antenna to sample the incident and reflected power (see Fig. 13). These couplers had a coupling factor of 37 db and a directivity of 37 db. With 7 kw peak power input, a pulse width of 1 μsec, and a PRF of 414 cps, the average RF power appearing at the active bolometer in the detector was approximately 0.5 mw. A short probe was used to sample the transmitted power (see Fig. 2). This probe was coupled to the remaining detector by a short section of *X*-band guide which also served as a high-pass filter to prevent stray coupling of the *S*-band beacon signals to the detector. The three detectors were assembled together, as shown in Fig. 13.

The test antenna was an open-end waveguide with the nose cone acting as the ground plane (see Fig. 14). The *E*-plane dimension of the waveguide was reduced from 0.4 to 0.1 inch, to create a narrow slot that would break down at 7 kw in the altitude range of 50,000 to 180,000 ft (Fig. 1). This reduction was accomplished in a combined transition section and *E*-plane bend made of stainless steel and terminated in a special flange containing a quartz window at the point of attachment to the side of the nosecone. This assembly was carefully tuned by means of tuning screws which were then locked in place to preserve the matched condition.

Breakdown tests were performed on the flight-model antennas in the laboratory vacuum chamber. Results of the tests on the antenna used in

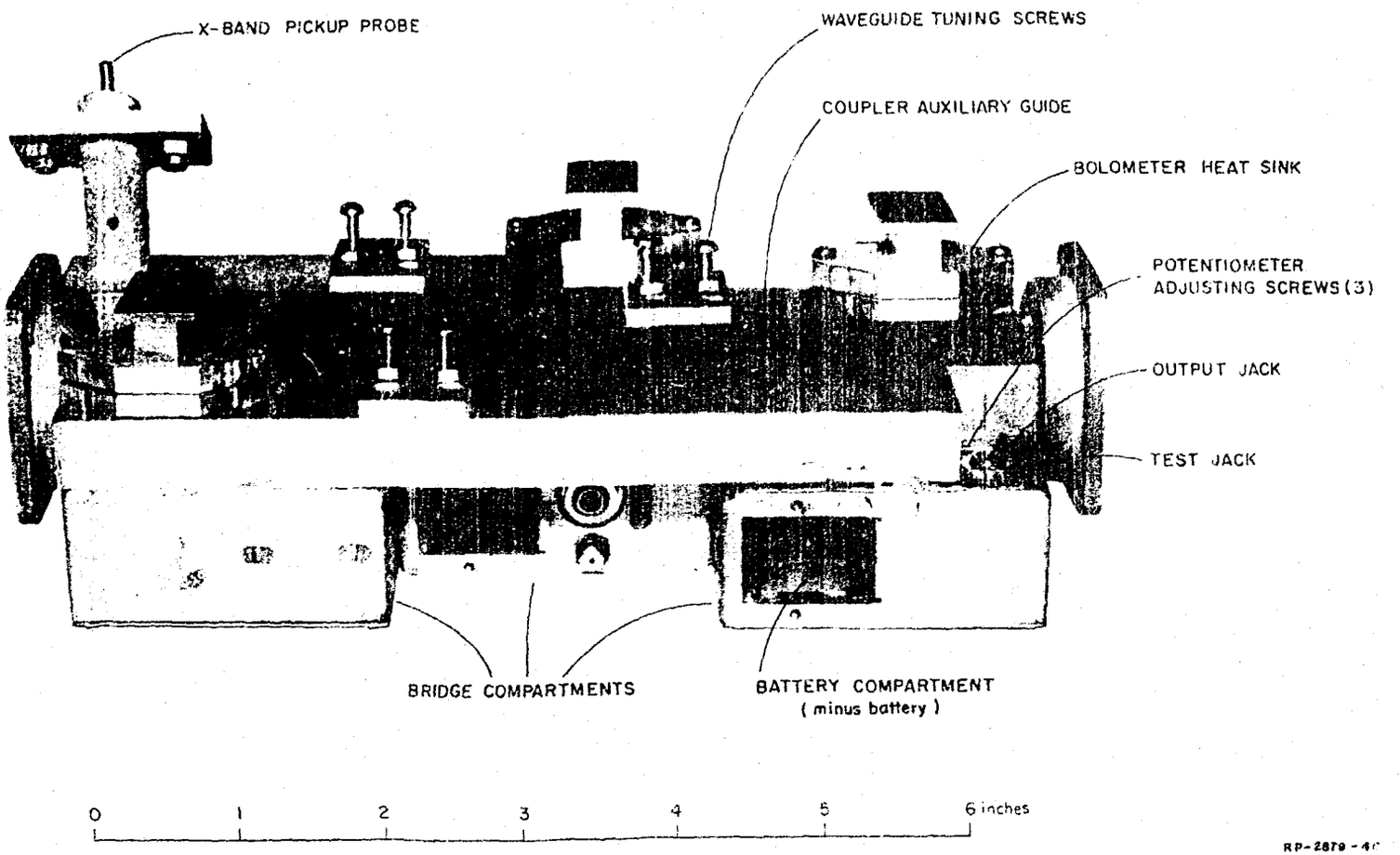

FIG. 13 COMPLETED X-BAND DETECTOR AND COUPLER ASSEMBLY

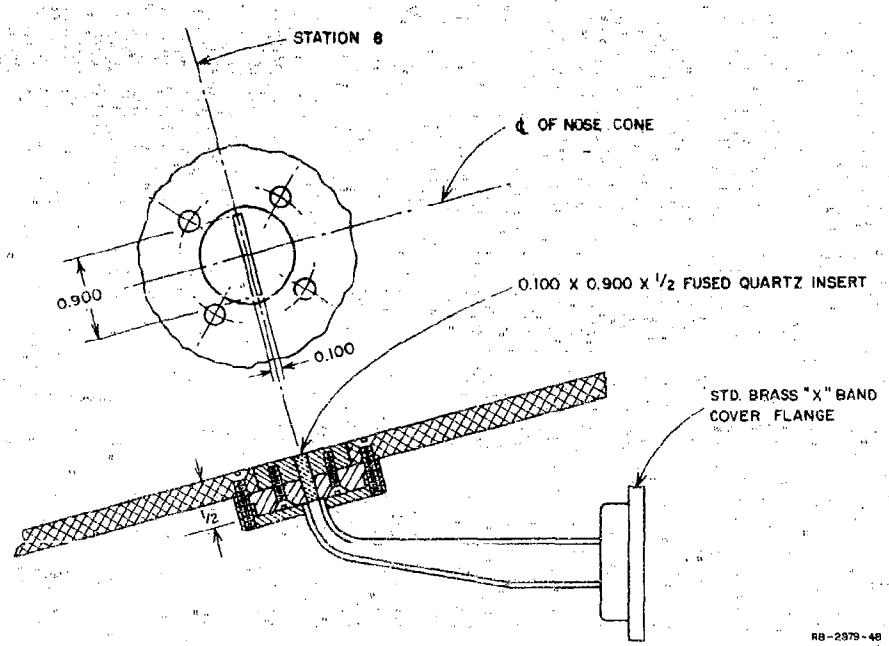

FIG. 14 X-BAND ANTENNA DETAILS

the 14 March firing are given in Figs. 15 and 16. Figure 15 shows the peak-power levels required to initiate and extinguish breakdown as a function of pressure. Waveforms of the reflected and transmitted pulses were obtained for several combinations of peak power and pressure by photographing oscilloscope traces of the video output. A sampling of these is presented in Fig. 16 with the corresponding points on the breakdown power curve indicated in Fig. 15. In all cases the pulse height was adjusted by means of attenuators to the same level for convenience in reading. Actual levels, in db relative to an arbitrary zero, are noted beside each pulse photograph. Figure 16(a) presents incident, reflected and transmitted pulse waveforms at various pressures at a peak incident power level of 9.4 kw. Figure 16(b) and 16(c) are for peak incident power levels of 5.9 and 1.5 kw, respectively.

When a step-function voltage is applied which is within the region above the curves of Fig. 15 a small but finite time is required for the electron density to build up enough to cause breakdown. The length of time required decreases with an increase of incident power at a constant pressure.[2] Also, at a constant input power the length of time required

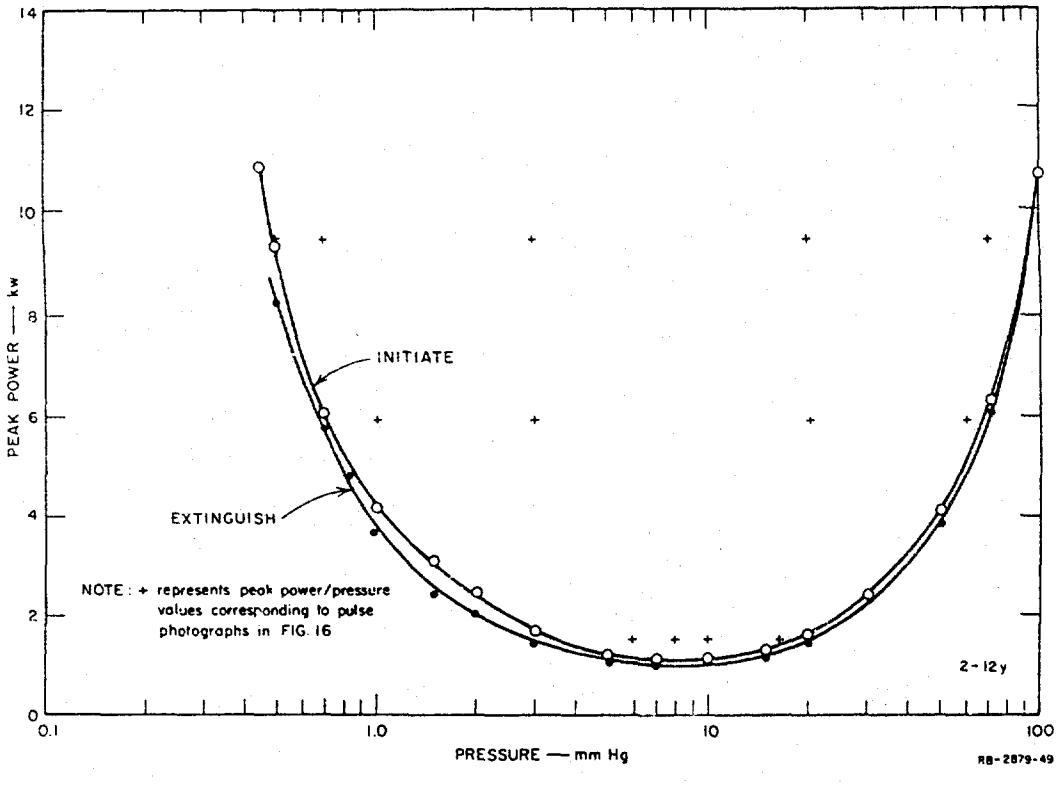

FIG. 15 X-BAND ANTENNA BREAKDOWN RESULTS – LABORATORY TEST

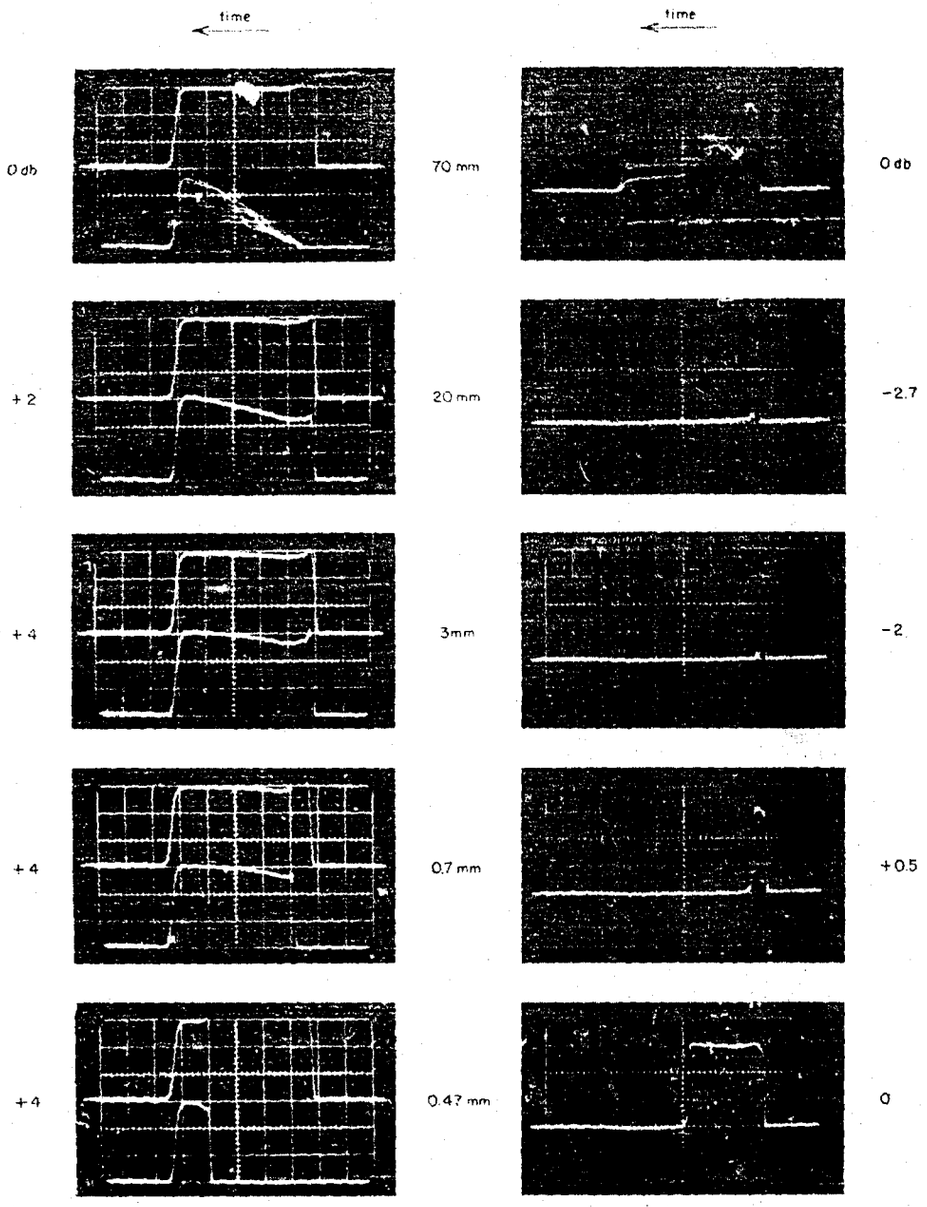

NOTES:

1. Peak power 9.4 kw
2. Frequency 9400 Mc
3. Pulse width 1 μsec
4. PRF 426 pps
5. Actual levels relative to initial level in db are shown at left and right sides.

(a)

RP-2679-56

FIG. 16 PULSE WAVEFORMS DURING BREAKDOWN OF X-BAND ANTENNA

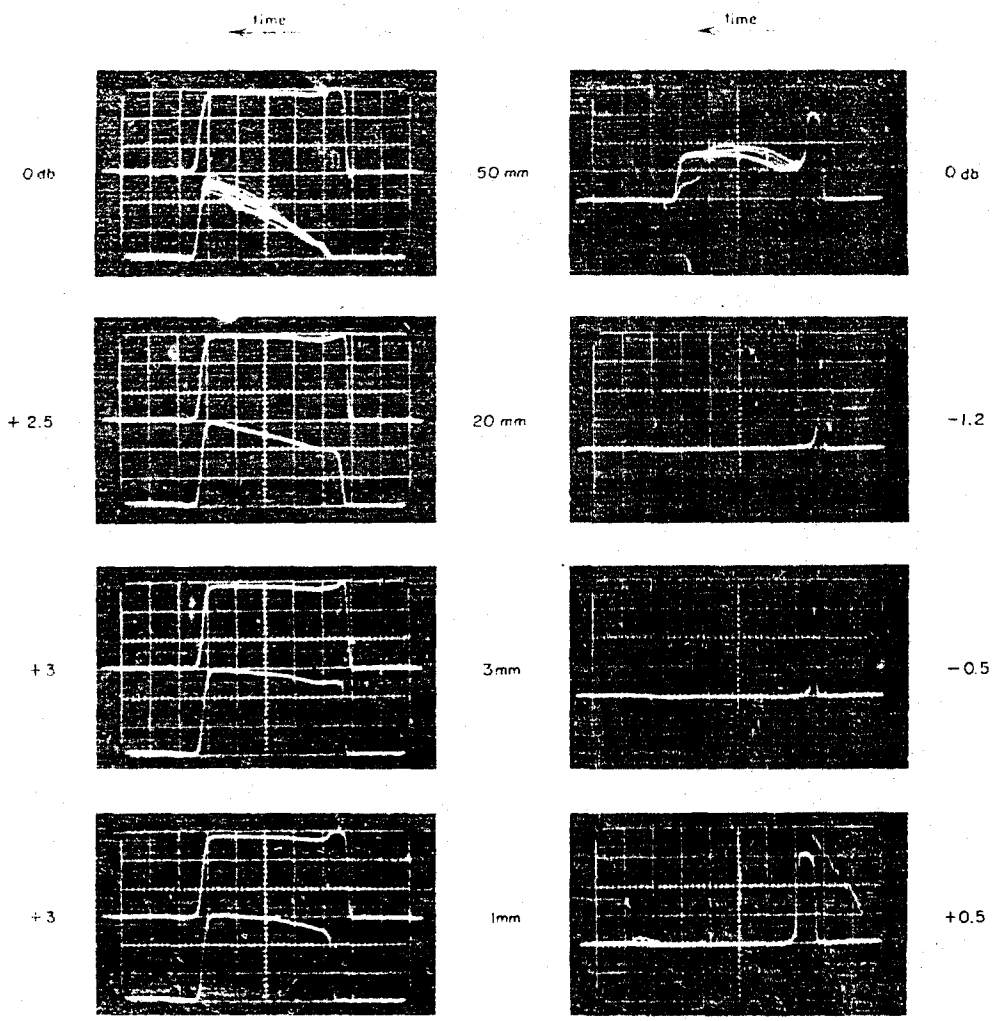

NOTES:

1. Peak power 5.9 kw
2. Frequency 9400 Mc
3. Pulse width 1 μsec
4. PRF 426 pps
5. Actual levels relative to initial level in db are shown at left and right sides

(b)

RP-2879-57

FIG. 16 (Continued) PULSE WAVEFORMS DURING BREAKDOWN OF X-BAND ANTENNA

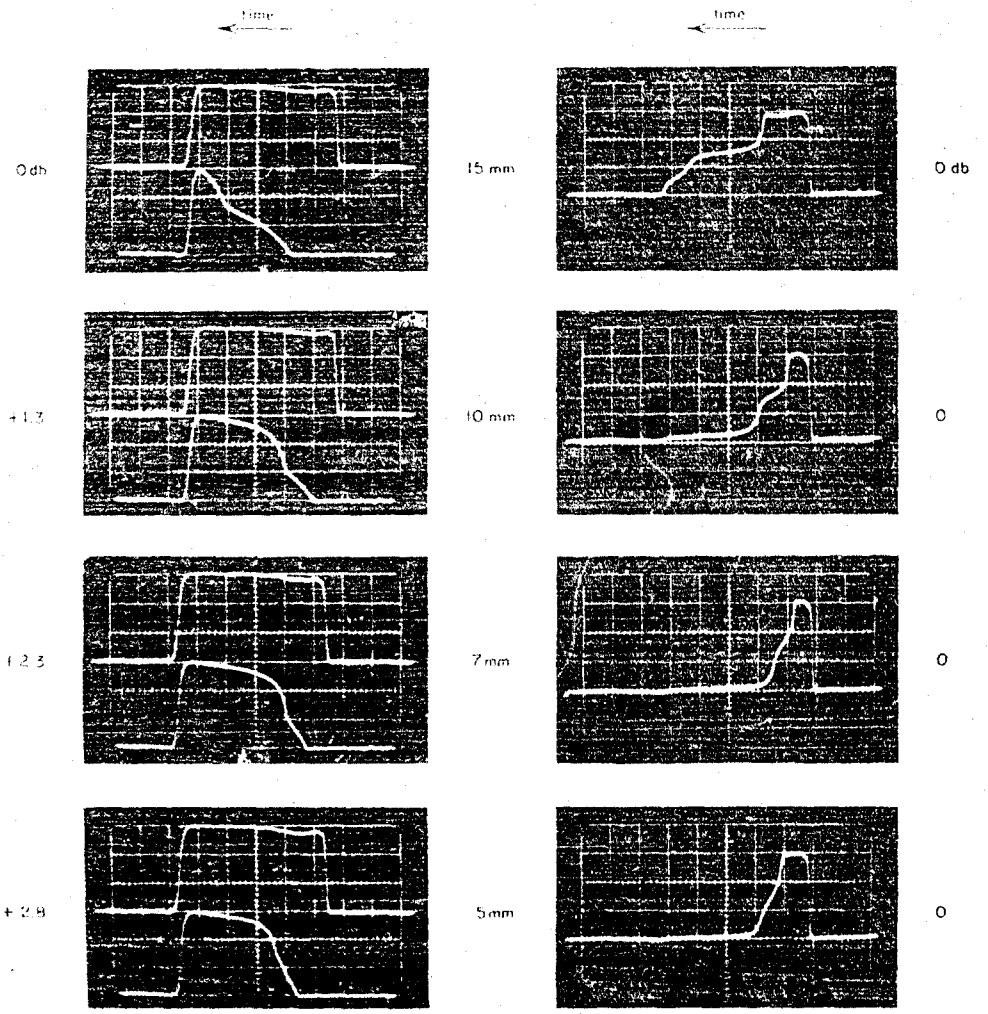

NOTES:

1. Peak power 1.5 kw
2. Frequency 9400 Mc
3. Pulse width 1 μsec
4. PRF 426 pps
5. Actual levels relative to initial level in db are shown at left and right sides

(c)

RP-2879-58

FIG. 16 (Concluded) PULSE WAVEFORMS DURING BREAKDOWN OF X-BAND ANTENNA

decreases with a decrease in pressure to approximately the pressure for minimum breakdown power. As the pressure is further reduced the time required increases again. The sequence of pulse shapes in Fig. 16 shows the widening and narrowing of the reflected and transmitted pulses as the pressure is varied.

C. TELEMETRY SYSTEM

The telemetry system was a standard FM/FM system with five subcarriers. Two of the subcarrier channels were commutated; the remaining three were uncommutated, or continuous channels. A summary of the characteristics is given in Table I. Channel A was used to monitor the

Table I

TELEMETRY SYSTEM CHARACTERISTICS

Frequency 234 Mc
RF power output—2 watts
Subcarrier channels:
(a) 22.0 kc ± 7½%—0-1 volt input, uncommutated
(b) 30.0 kc ± 7½%—0-1 volt input, uncommutated
(c) 40.0 kc ± 7½%—0-1 volt input, uncommutated
(d) 52.5 kc ± 7½%—-0.2 to +0.8 volt input, commutated
(e) 70.0 kc ± 7½%—-0.2 to +0.8 volt input, commutated

output of the pressure gauge; Channels B and C were used to monitor the VLF receiver data; and Channels D and E were used to monitor several data channels on a time-sharing basis. The schedule of data for Channels D and E was as follows:

CHANNEL D

FUNCTION	SAMPLING RATE
VLF magnetometer data	20 samples per sec
VLF antenna calibration—Channel 1 data	20 samples per sec
VLF antenna calibration—Channel 2 data	20 samples per sec
VLF receiver temperature data	20 samples per sec
Field strength data—Channel 1	10 samples per sec
Field strength data—Channel 2	10 samples per sec
6.3-volt d-c monitor data	20 samples per sec
28-volt d-c monitor data	20 samples per sec
150-volt a-c monitor data	20 samples per sec
1-cps modulation voltage monitor data	20 samples per sec
Thermocouple reference monitor data	20 samples per sec

Channel E

FUNCTION	SAMPLING RATE
X-band antenna incident power data	40 samples per sec
X-band antenna reflected power data	40 samples per sec
X-band antenna transmitted power data	40 samples per sec
VHF antenna incident power data	40 samples per sec
VHF antenna reflected power data	30 samples per sec
VHF antenna transmitted power data	30 samples per sec
Surface temperature data (4 channels)	10 samples per sec (each channel)

Figure 17 is a block diagram of the telemetry system. A three-section mechanical commutator was used to commutate the 52.5- and 70-kc channels, as shown. The amplifier feeding the 70-kc SCO (subcarrier oscillator) was used to raise the voltage level of the data channels from the range of 0 to 1.6 mv to the input range of 0 to 0.8 volt of the SCO. A negative pedestal voltage equal to 20 percent of full-scale was applied to every other commutator segment in both the 52.5- and 70-kc channels to permit synchronization of the automatic decommutation systems at the telemetry ground stations. In addition, three consecutive commutator segments were connected to each other and to a positive full-scale voltage to provide a frame synchronization signal and a full-scale calibration point for each revolution of the commutator. Similarly, zero and half-scale calibration points were also employed. The outputs of the five SCO's were combined in a linear isolation network and used to frequency-modulate the transmitter. Figures 18 and 19 show the configuration of the telemetry package, which was mounted on both sides of an aluminum mounting plate located between Stations 33.5 and 42.5.

D. POWER SUPPLY

Figure 20 is a block diagram of the internal power supply used to power the rocket instrumentation package. The internal battery consisted of five Yardney PM-5 cells and fifteen Yardney HR-3 cells connected in series to form a 28-volt d-c supply with a 6.3-volt tap. The changeover relay was used to transfer the instrumentation load to an external battery, thereby conserving internal battery power until just prior to flight.

Changeover, as well as other functions described in the following paragraphs, was performed by remote control from the blockhouse. A control panel specially designed for this purpose by the Institute was located in

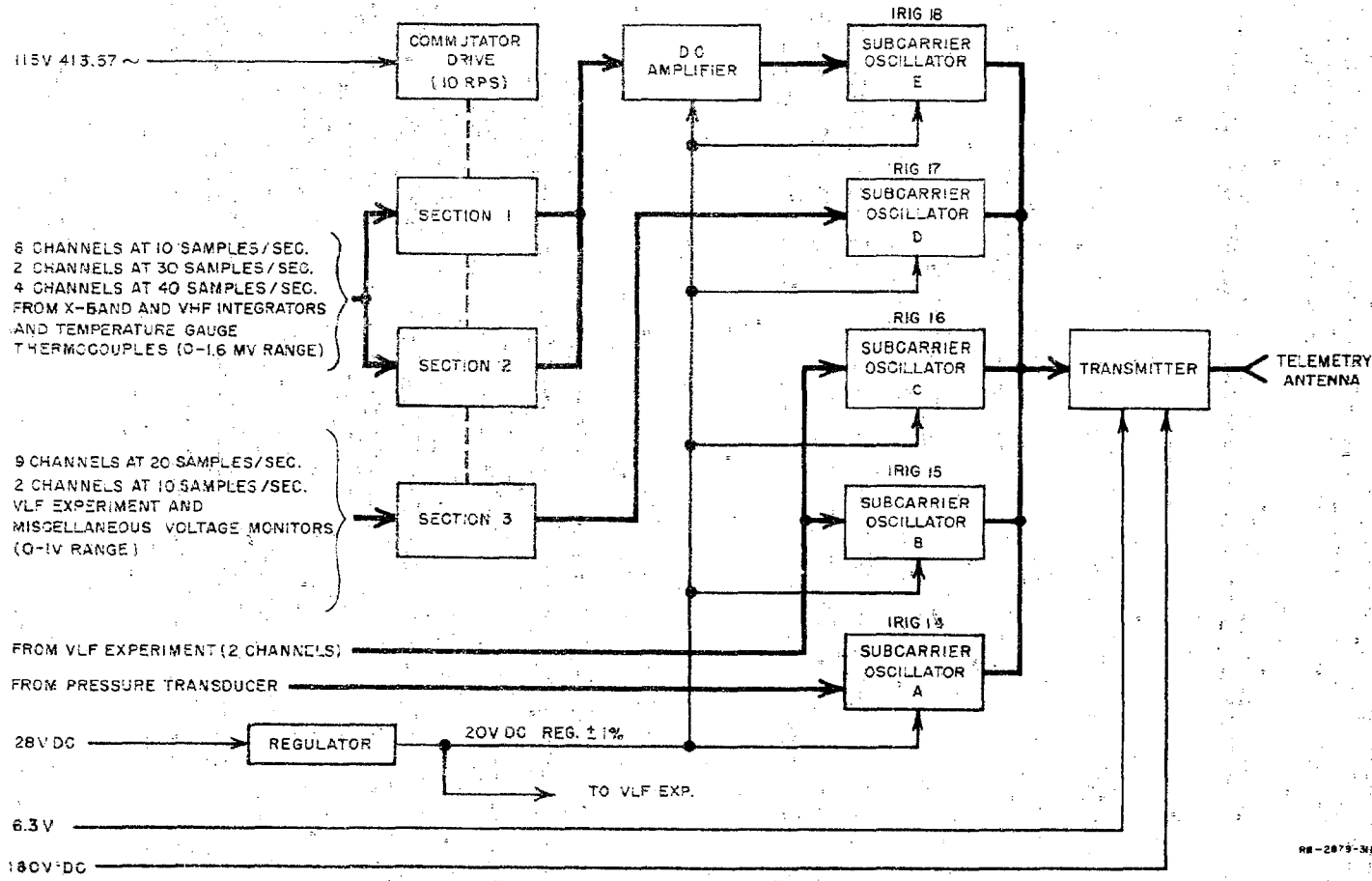

FIG. 17 BLOCK DIAGRAM OF TELEMETRY SYSTEM

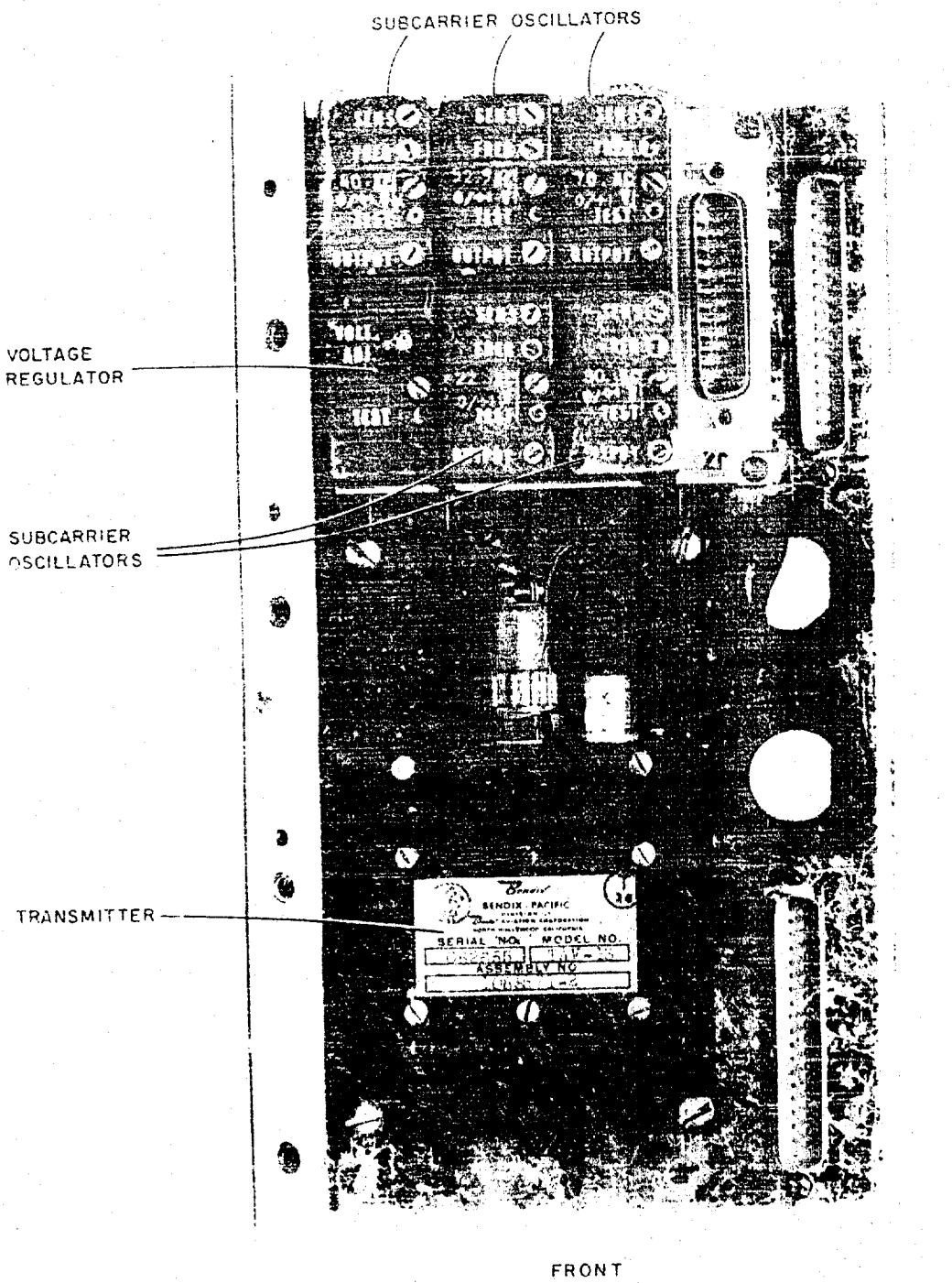

FIG. 18 COMPLETED TELEMETRY PACKAGE – FRONT VIEW

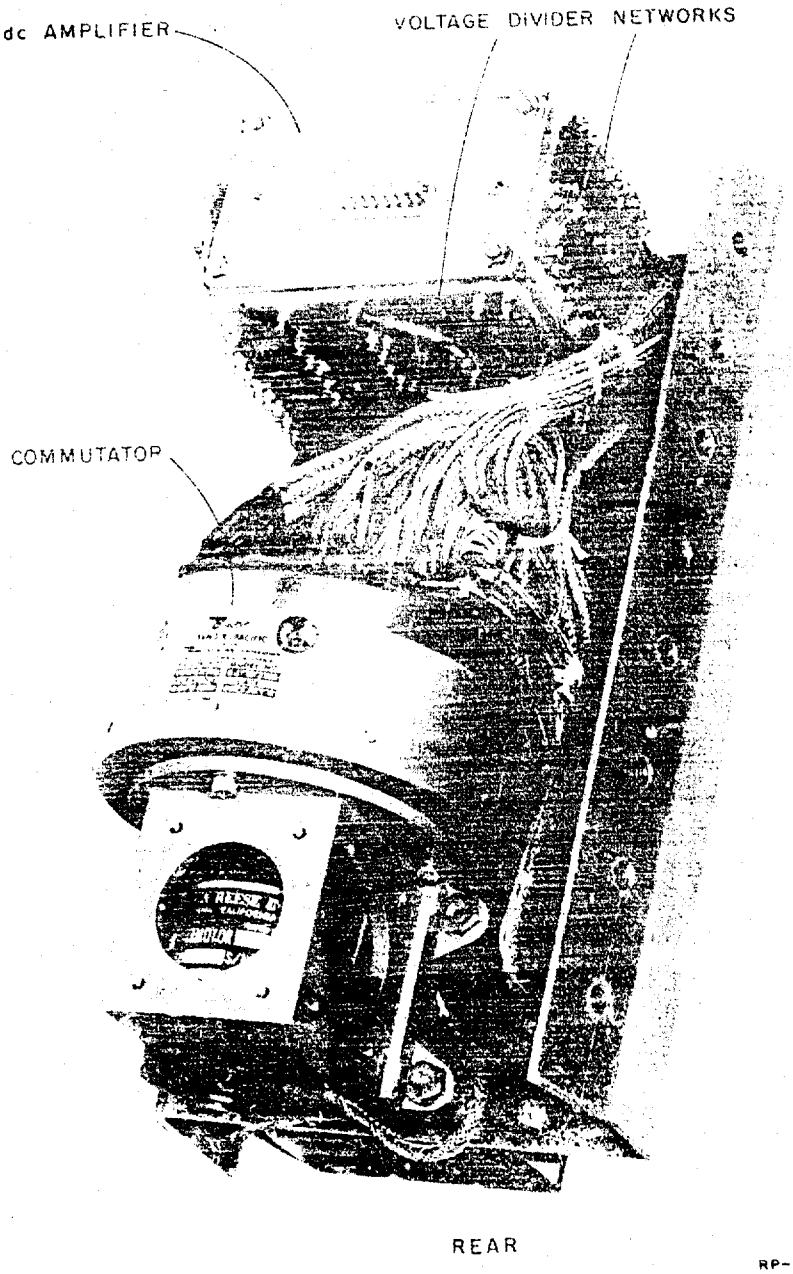

FIG. 19 COMPLETED TELEMETRY PACKAGE – REAR VIEW

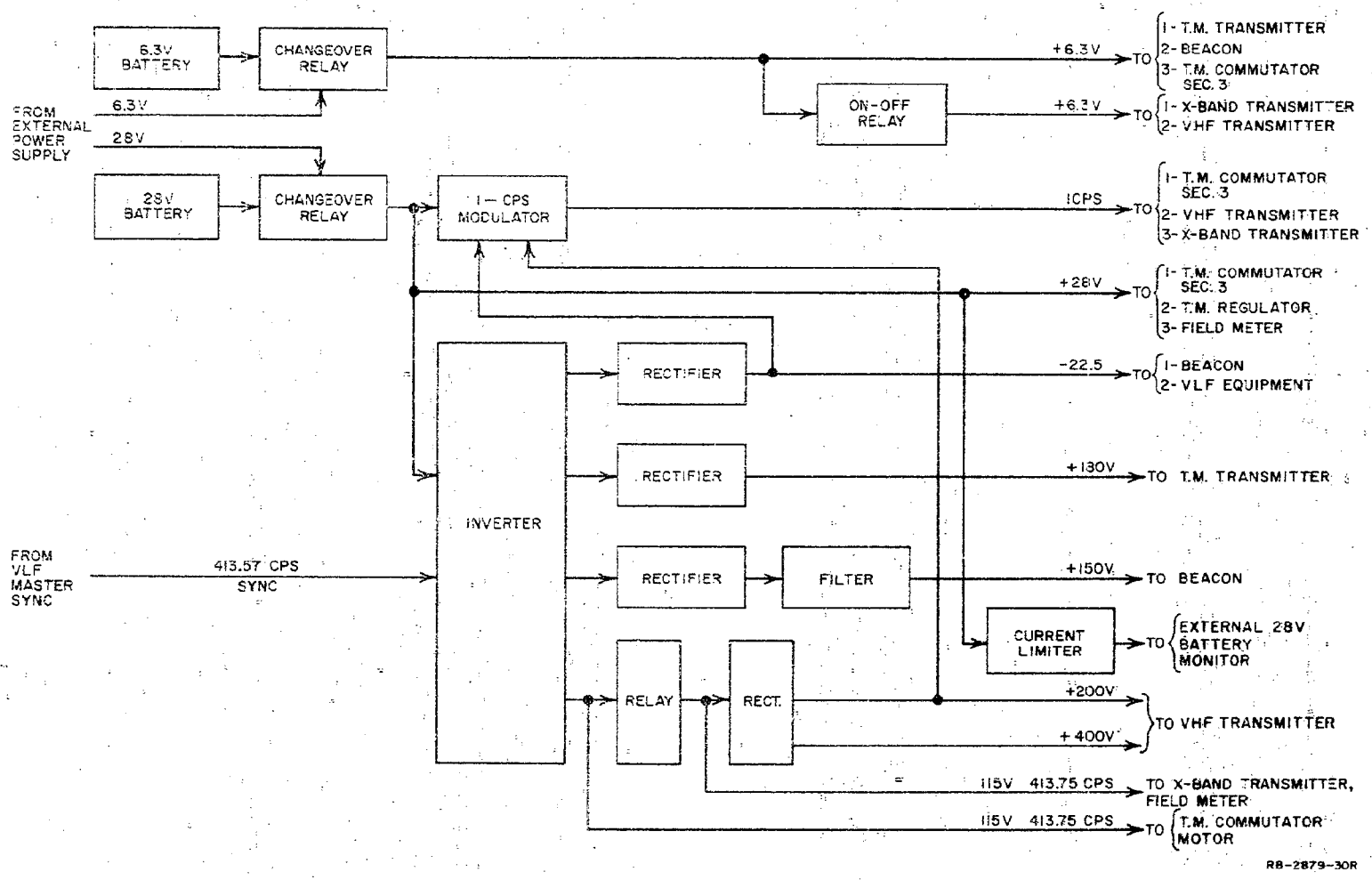

FIG. 20 BLOCK DIAGRAM OF COMMON POWER SUPPLY

the blockhouse and tied into a cable system which terminated at a junction box on the launch rail. Two umbilical cables were connected to the rocket instrumentation package and to the junction box on the rail, completing the remote control circuits. Figure 5 shows the receptacles for the umbilical cables.

The transistorized inverter was triggered to run at a constant frequency of 413.57 cps. This wa a requirement of the VLF instrumentation mentioned in Sec. I. As a part of this investigation, a dual receiver operating at 15.5 and 18.0 kc was mounted in the instrumentation package to record VLF signal strength. Because of the high sensitivity of the receiver and the relatively low frequencies to be detected, it was necessary to prevent harmonics of the power supply and the *X*-band pulse networks from occurring at these frequencies. The 413.57-cps rate met this requirement.

The power supplied to the *X*-band and VHF transmitters was controlled by relays which were energized by remote control from the control panel at blockhouse. This was necessary to permit filaments to be heated before plate voltages were applied.

The 28-volt, 6.3-volt, and 20-volt bus voltages, and the 1-cps modulation voltage were monitored at the same panel.

E. ENVIRONMENTAL SENSORS

1. Temperature

Surface temperatures were measured by means of thermocouple units installed at the locations shown in Fig. 2. This arrangement permitted measuring the surface temperature of each test antenna, as well as obtaining a profile of temperature along the surface of the instrumentation package. Each unit consisted of a Chromel/Alumel junction imbedded in a ¼-inch diameter threaded plug which screwed into the rocket skin. The plug material was the same as that of the rocket skin, with the exception of the plug located at Station 8. Table II summarizes the important features; as shown the temperatures were measured very close to the surface, since the temperature of the layer of air adjacent to each test antenna was of primary interest.

Table II

THERMOCOUPLE DATA

STATION LOCATION	ROCKET SKIN MATERIAL	PLUG MATERIAL	DEPTH OF JUNCTION BELOW SURFACE
0	Stainless steel 303	S.S. 303	0.002 inch
8	Magnesium alloy AZ91C-T6	S.S. 303	0.002 inch
16	Aluminum alloy 6061T6	Al. 6061T6	0.004 inch
42.5	Aluminum alloy 6061T6	Al. 6061T6	0.004 inch

The output voltages were sampled by the commutator as described in Part C, amplified, and telemetered to the ground recording stations. Reference junctions were located on a terminal board at approximately Station 16, where the Chromel/Alumel gauge leads were joined to copper wires going to the commutator. An iron/Constantan thermocouple was attached to the board, with its leads going via the pull-away cables to a 32°F reference junction on the launch rail. The output of this thermocouple, read at the blockhouse, provided a means of determining the temperature of the reference junctions of the four surface-temperature thermocouples at the time of launch. A simple heat-sensitive resistance circuit was also attached to the board to measure any drift in the temperature of the reference junctions after launch. The output of this device was sampled and telemetered to the ground stations.

2. Pressure

Surface pressure was measured at Station 8, which was the location of the *X*-band antenna (Fig. 2). An ionization type of gauge was used, since this was the only type of gauge small enough to fit into the limited space available and still be capable of covering the pressure range of from 200 to 0.5 mm Hg in one step.* This range includes the range of pressures expected during breakdown of the *X*-band antenna. The output of the gauge was a series of 10-volt pulses, approximately 100 μsec wide. The pulse repetition rate was a function of the pressure, and varied from about 250/sec at 200 mm Hg to about 1/sec at 0.5 mm Hg. These pulses were fed through a pulse-widening network to a separate subcarrier oscillator and telemetered to the ground. Pressure was determined by counting the number of pulses in a given time interval.

* The minimum pressure which can be measured depends on the rate of change of pressure and the desired accuracy. This is discussed in Sec. III-C-3.

F. VLF EXPERIMENT

The VLF experiment consisted of flight measurements of the signal strength of VLF transmissions from Stations NSS and NBA (15.5 and 18.0 kc) as a function of altitude. Because of the extremely long wavelength in comparison with the dimensions of the rocket, it was necessary to use the rocket itself as a short dipole to obtain the longest possible antenna. This was accomplished by inserting a dielectric coupling between the instrumentation package and the Cajun rocket, and connecting the VLF receiver input terminals across the gap thus formed.

A duplicate receiver was located on the ground at the telemetry station near the launch site to provide simultaneous reference signals that would allow later correction for variations in transmitted power

Since the antenna impedance would be changed by the presence of ionospheric plasma it was necessary to sample the antenna impedance continuously and telemeter this data to the ground to allow for later correction of the signal strength data. Another modifying influence was the directional pattern characteristics of the dipole antenna. In order to correct for pattern effects a magnetometer was included in the airborne instrumentation to determine the approximate attitude of the rocket throughout the flight. These data were also sampled and telemetered to the ground.

G. STATIC FIELD MEASUREMENT

Included in the instrumentation was a generating-voltmeter type of field meter that measured the magnitude of the electric field existing at a point on the skin of the rocket 2 inches aft of the nose cone. The main objective for the field-meter experiment was the investigation of the effects of the rocket engines in charging the vehicle. One of the design goals, therefore, was that the field meter amplifiers be sufficiently rugged and free of microphonics to be able to function during periods of burning. For this reason, transistors rather than tubes were used in the amplifier. To achieve maximum dynamic range with minimum complexity a linear amplifier-detector circuit was chosen. The amplifier used in the tests had a dynamic range of 40 db. In order to remain within the dynamic range of the telemetry system without the necessity of complicated switching, two telemetry channels were used simultaneously to transmit field-meter information. Channel 1 was fed the full output voltage from the detector,

while Channel 2 was fed one-tenth the detector output voltage. Thus, at high signal levels (fields up to roughly 100 kv/meter) Channel 2 was within its linear range and Channel 1 was saturated, while at low field levels Channel 1 was within its linear range and Channel 2 indicated zero.

The detector head mounted in the skin of the vehicle (Fig. 5) was of conventional design. A set of grounded vanes alternately covered and uncovered a set of stationary vanes, thereby periodically exposing the stationary vanes to the external electric field. The alternating current generated in the stationary vanes by this periodic exposure to the electric field was proportional to the magnitude of the field. This signal was fed to the input of the amplifier-detector circuit. It should be noted that a simple system of this sort does not indicate the polarity of the field. Also, the signal produced by the interruption of ion or electron current flow to the stationary vanes is indistinguishable from the signal produced by the electric field. (A current density of 35 $\mu a/m^2$ produces the same reading as a field of 1 kv/meter).

II. BEACON

An S-band beacon, Type AN/DPN-41, was carried in each package to assure good radar tracking throughout the flight. Space requirements precluded the use of the standard beacon power supply. Instead, power was obtained from the common power supply and fed to the beacon through specially designed filters and shielded cables to prevent spurious triggering of the beacon by stray pickup on the power leads. Standard quadraloop beacon antennas were mounted one on each side of the equipment package, as shown in Fig. 2. The beacon transponder was mounted in the forward section between Stations 11 and 20.

I. GROUND INSTRUMENTATION

1. General

Figure 21 shows the location of ground stations used for the launchings at Eglin Gulf Test Range. The launch site, Site A-11, Radar Station A-13, and Telemetry Station A-6 are all located within five miles of each other on Santa Rosa Island, just off the Florida coast. Firings are directed toward the Gulf of Mexico from the seaward side of Santa Rosa Island. A second radar station and a second telemetry station are located southeast

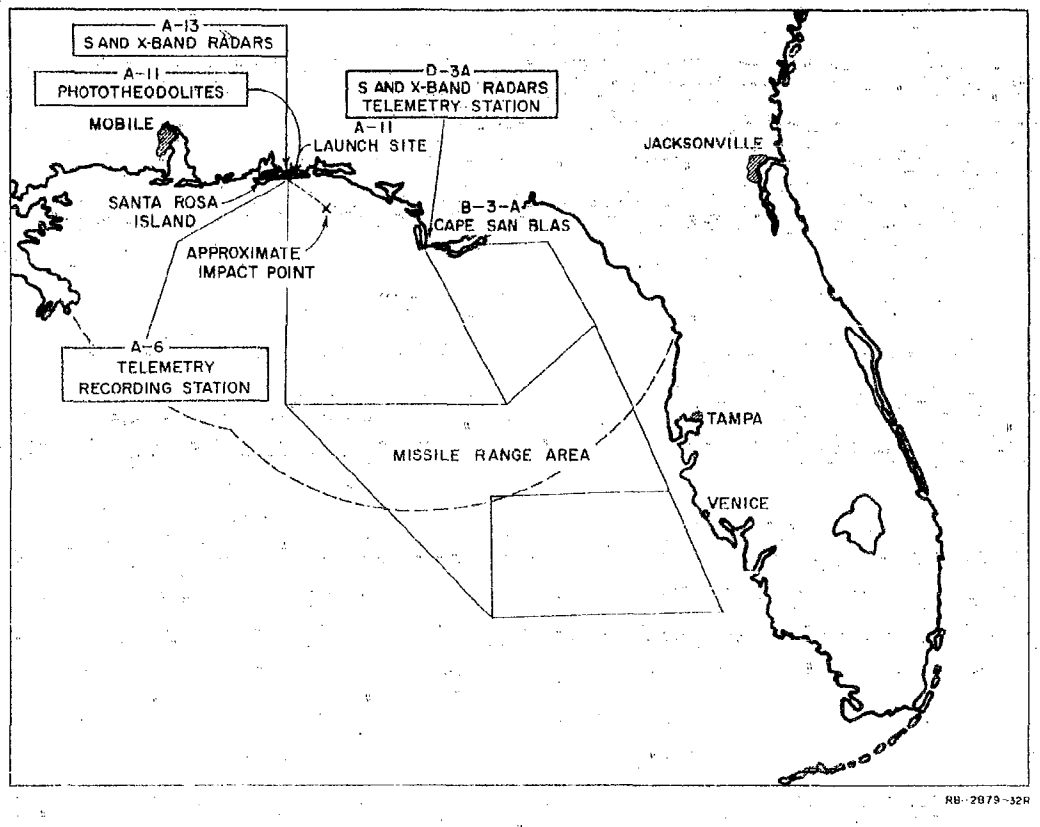

FIG. 21 MAP OF EGLIN GULF TEST RANGE

of the launch site at Cape San Blas, a distance of about 100 miles. The facilities of both Santa Rosa Island and Cape San Blas were employed in the three launchings to ensure continuous data in spite of changing attitude of the rocket in flight.

2. *X*-Band

Receiving systems were employed at Sites A-13 and D-3 to detect and record the shapes of the pulses radiated by the *X*-band test antenna. The antennas were parabolic dishes with a gain of 44 db and used fixed, circularly polarized feeds. Antenna positioning data for the *X*-band antennas was obtained from the nearby *S*-band tracking radars. The video output of each receiver was displayed on an oscilloscope and photographed continuously by a strip camera throughout the flight.

The fine details of the changes in pulse shape during breakdown were of primary interest. Consequently, because the pulse widths had a maximum value of 1 μsec and a probable minimum value of 0.1 μsec, the IF and video bandwidths were increased to 20 Mc and 10 Mc, respectively, to eliminate waveform distortion which would otherwise occur in passing through these units. AGC, with a time constant of a few milliseconds, was employed to keep the amplitude of the displayed pulses approximately constant, so that they could be analyzed in detail. The strip cameras were synchronized to photograph every tenth pulse, which was considered adequate for analysis.

3. VHF

VHF receivers were used at Sites A-6 and D-3 to receive the signals radiated by the VHF test antenna. The AGC voltage was fed into a Sanborn recorder to provide a record of VHF signal strength. The expected fluctuations in signal strength caused by antenna breakdown are relatively fast compared with those caused by changing antenna orientation and changing range, and could therefore be distinguished.

4. Telemetry

Standard FM/FM telemetry equipment was employed at Sites A-6 and D-3 to receive and record the telemetered signals. Five subcarrier discriminators were employed at 22, 30, 40, 52.5, and 70 kc, all with ±7 ½% bandpass filters. The output of each discriminator was recorded, as well as the composite of the five channels, the receiver AGC voltage, and the data channel outputs of the automatic decommutator in the case of the 52.5 and the 70-kc channels. Other data, which were not telemetered but recorded on telemetry tape and Sanborn recorders, consisted of the VHF receiver AGC voltage, mentioned in Sec. II-I-3, and the VLF ground-receiver output voltages (Site A-6 only, see Sec. II-I-5).

5. VLF

A dual VLF receiver was located at a point about 300 feet from the telemetry station at Site A-6 to receive signals from NSS and NBA for reference purposes. The outputs of this receiver were transmitted through 50-ohm coaxial cable to recorders in the telemetry station (see Sec. II-I-4).

6. Tracking

S-band radars located at Sites A-6 and D-3 were used to track the beacon in the rocket. In addition, optical tracking data were supplied for approximately the first 30 seconds of flight by phototheodolites located at Site A-6.

J. SHOCK AND VIBRATION TESTING

Shock and vibration tests were performed on completed instrumentation packages Nos. 2 and 3. Equipment employed in these tests consisted of a Barry Model 150 VD shock machine, which is essentially a drop-testing machine, and an M-B Model C-25 vibration test machine. The instrumentation packages were so mounted that the shock and vibration forces were parallel to the longitudinal axis. Since only the actual flight packages were available for test, it was not possible to test to destruction.

Table III lists the test conditions imposed on the two equipment packages. Electronic parts and hardware items that showed a tendency to loosen were secured by potting compounds or mechanical locking devices. No major damage resulted from these tests.

Table III

ENVIRONMENTAL TEST CONDITIONS

TEST	DESCRIPTION OF TEST	
	Package 2	Package 3
Shock 1	8-inch drop, 25g, 10 ms duration	7.25-inch drop, 25g, 11 ms duration
Shock 2	24-inch drop, 50g, 11 ms duration	24-inch drop, 50g, 11 ms duration
Shock 3	3-inch drop, 10g, 11 ms duration	2.5 -inch drop, 10g, 11 ms duration
Vibration 1	20-125 cps, 5g, 1 minute	10-30 cps, 1g, 2 minutes
Vibration 2	125-500 cps, 5g, 1 minute	30-70 cps, 0.036-inch amplitude 2 minutes
Vibration 3	100-500 cps, 8g, 1 minute	70-500 cps, 5g, 2 minutes
Vibration 4	--	100-500 cps, 8g, 2 minutes

III FLIGHT TEST RESULTS AND ANALYSIS

A. SUMMARY

The launch site was Site A-11, Aerospace Launching Facility, Eglin Gulf Test Range, Santa Rosa Island, Florida. The launchers were the general-purpose type, designed so that both of the Nike launching tees release simultaneously from the launcher after the vehicle has traveled 200 inches along the rail. Umbilical cables were pulled from the payload at first motion. Launch time is defined as the time of first-stage ignition, as observed from phototheodolite film. Table IV gives times of pertinent events for the three flights.

Table IV

LAUNCH DATA

Mission Number	1	2	3
Date	4 Nov. 1960	14 March 1961	24 March 1961
Launch Time (Zulu)	2052:00.390	2152:00.535	1917:59.367
1st Stage Separation (sec)	-	3.5	3.6
2nd Stage Ignition (sec)	16.67	18.265	19.6
2nd Stage Burnout (sec)	-	21.535	22.966
Radar Tracking Data (sec)	54.5	316.0	none
Phototheodolite Data (sec)	19.67	27.3	23.1
Elevation Angle	-	86°	-
Azimuth Angle	-	154°	-

Additional data on ground-support equipment, vehicle trajectories, wind velocities, and launch facilities are available from Ref. 6.

B. FIRST FLIGHT--ROCKET AA6.800

Rocket AA6.800 was launched from Eglin Gulf Test Range on 4 November 1960. Radar and camera records show that the rocket performed as expected. A malfunction occurred in the instrumentation power supply causing all equipment to temporarily cease operating during the Nike burning period and to permanently cease operating at Cajun ignition approximately 16.7 seconds after launch.

The *X*-band transmitter was being monitored prior to launch and was functioning. Immediately following launch, however, the *X*-band transmitter was reported to have stopped, and it is presumed to have stayed off until $t = 3.112$ seconds, when the telemetry returned and showed it to be functioning again. It is believed that the radar beacon also came back on when the rest of the systems did, because the proper supply voltages to the beacon were indicated by the telemetry system. No report of the beacon having returned to operation was received; however, this was probably due to the fact that the radar which was interrogating the beacon was unable to reacquire the rocket after losing it at launch. Another radar did skin-track the Cajun to about 200,000 feet before it lost contact.

All available information indicates that a malfunction occurred in the power supply while accelerating during Nike engine burning. The fault was apparently cleared when the acceleration was removed at Nike burnout, and all systems appeared to function properly again until Cajun ignition occurred at $t = 16.7$ seconds, at which time the malfunction reappeared and remained. The power supply is the only point in the system in which a malfunction could cause all systems to go on and off at the same time. The exact location of the fault in the power supply is impossible to determine. However, it is felt that because all systems failed together it must have occurred at the input side of the inverter, where the 28-volt battery voltage is chopped to produce the 414-cps wave that supplies all the ac-to-dc converters, as well as the 414-cps loads.

C. SECOND FLIGHT- ROCKET AA6.801

1. Rocket Performance Data

Rocket AA6.801 was launched from Eglin Gulf Test Range on 14 March, 1961. Figure 22 shows the complete rocket assembly mounted on the launching rail and raised to the firing position. Radar camera records show that the rocket performed as expected. Figure 23 shows velocity, acceleration, and altitude for this flight. No data were obtained from the *X*-band experiment due to a failure of the transmitter shortly after launch. Data were obtained from the environmental sensors, the VHF experiment, the field strength experiment and the VLF experiment. These are described in the following paragraphs.

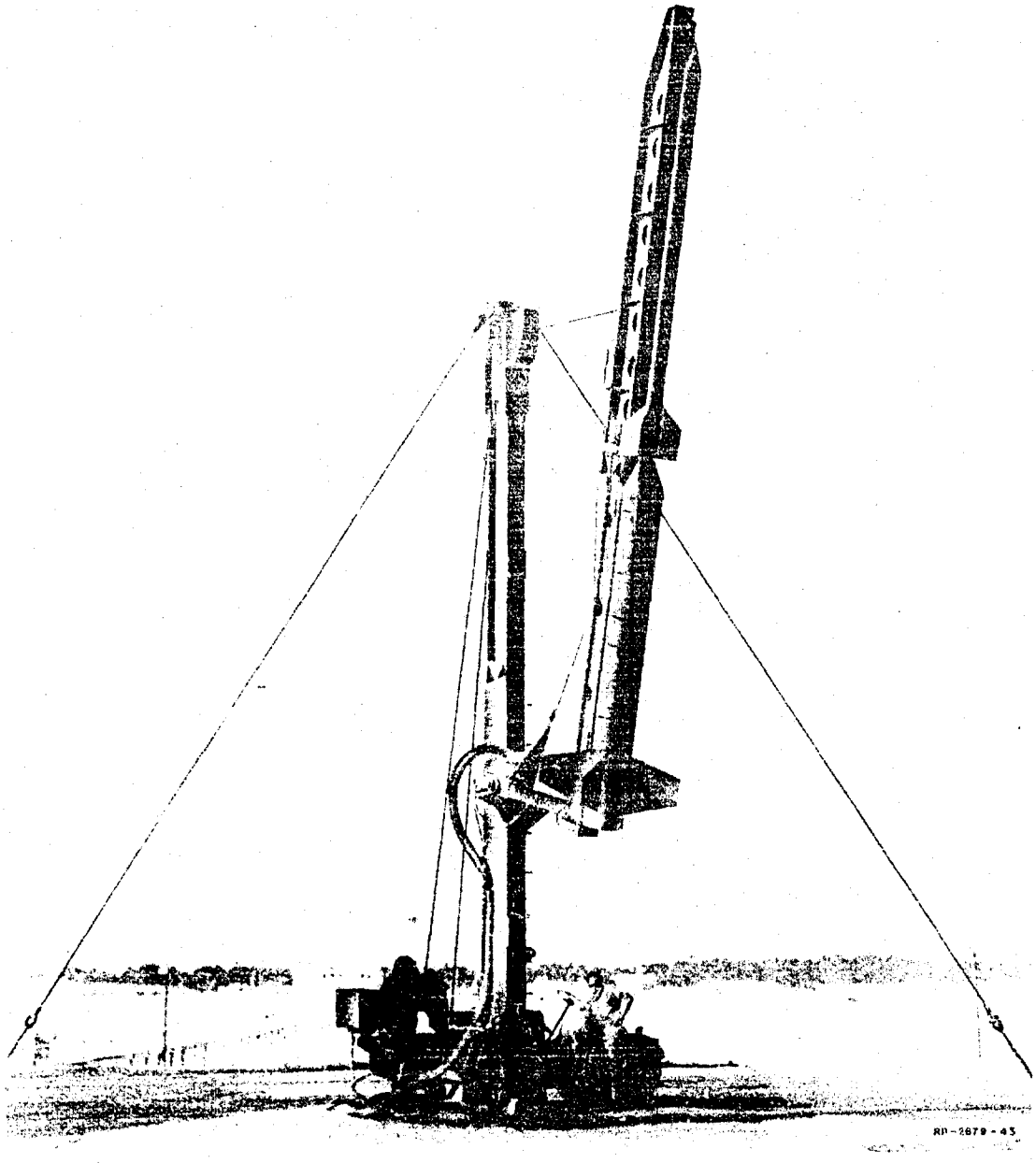

FIG. 22 NIKE-CAJUN ROCKET ON LAUNCH RAIL

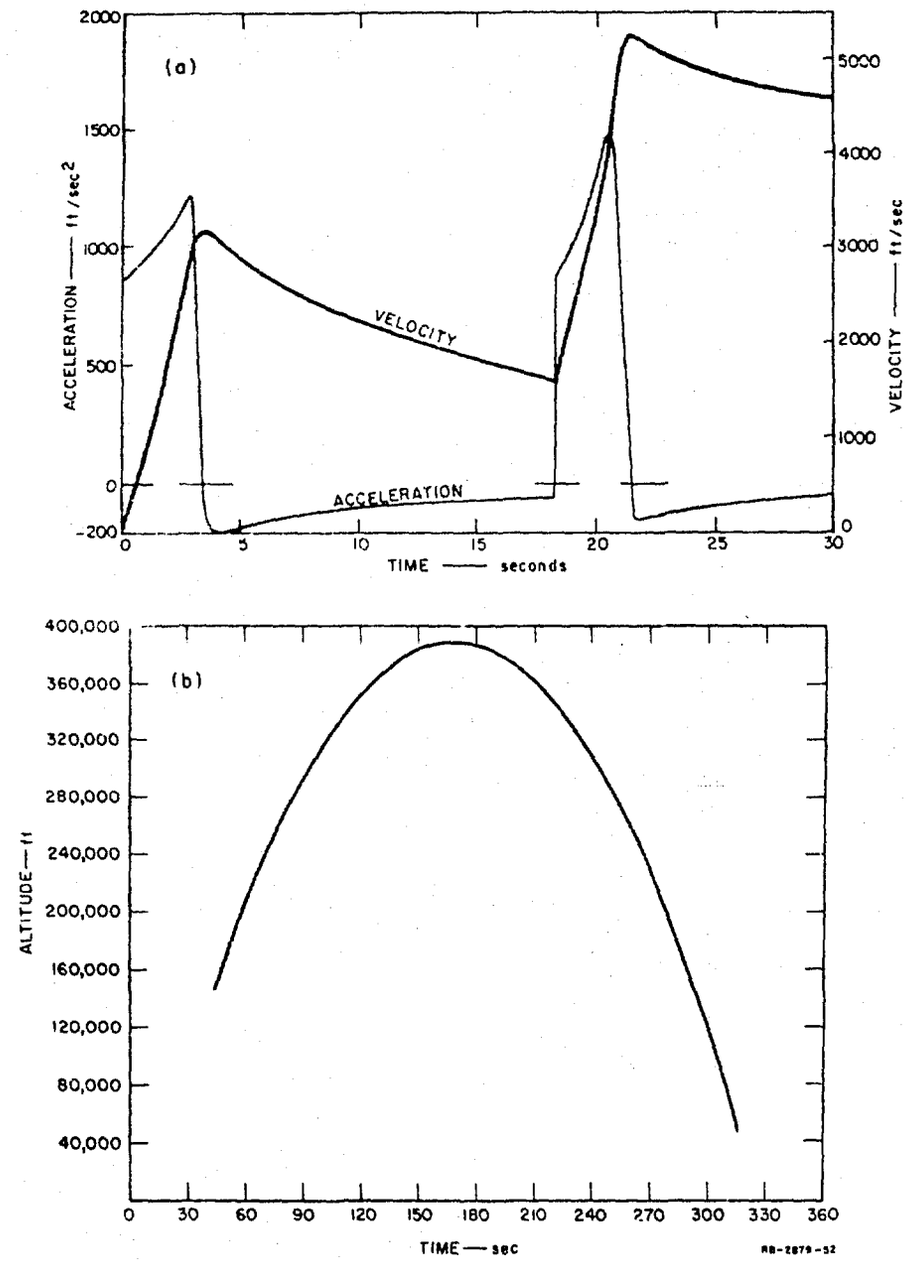

FIG. 23 VELOCITY, ACCELERATION, AND ALTITUDE vs. TIME – ROCKET AA6.801

2. Skin Temperature

A graph of the measured temperature data is given in Fig. 24. In general the surface temperatures were well below the design values, thereby allowing a greater margin of safety than was planned. Note that these are external surface temperatures, and are probably appreciably higher than those on the inside of the rocket due to thermal time lag and the relatively short flight time. Temperature peaks occurred shortly after the velocity peaks, as would be expected. Near the peak of the trajectory the temperature profile was almost constant at about 200°F. This condition continued through the peak and subsequent descent until denser air was re-entered at about 150,000 feet, at which time temperatures again rose to high values, though not as high as during rocket burning. The temperature at the tip of the nose cone during this re-entry reached a maximum of 500°F at an altitude of 40,000 feet and a velocity of 4200 ft/sec.

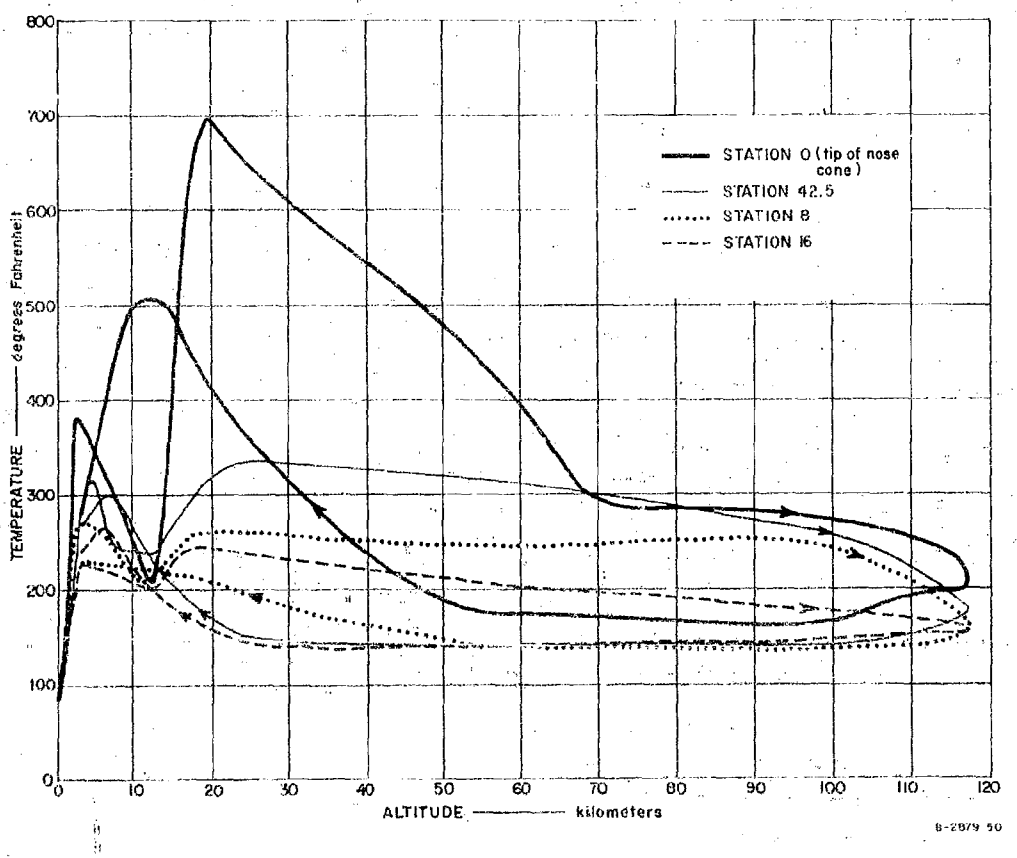

FIG. 24 SURFACE TEMPERATURES vs. ALTITUDE AND TIME -- ROCKET AA6.801

3. Surface Pressure

Pressure data which were obtained from the ionization gauge at the *X*-band antenna location (Station 8) is shown in Fig. 25, together with the calculated values of pressure. The ambient free-stream pressure, obtained from the ARDC 1959 standard atmospheric model[7] is also shown in Fig. 25. The pressure on the nose cone due to aerodynamic effects was calculated from the following equation:*

$$P_2 = P_1 \left[1 + \frac{\gamma M_1^2}{2} - \frac{\Delta P}{q} \right] \tag{6}$$

where

γ = ratio of specific heats†

P_2 = pressure along the conical surface of the nose cone

P_1 = ambient free-stream pressure

M_1 = free-stream Mach number.

The ratio $\Delta P/q$ as a function of the Mach number was obtained from Taylor and Maccoll's curves[8] for a semi-vertex angle of 14.5 degrees. These are valid as long as the shock wave is attached to the rocket, the condition existing in the altitude region for which P_2 is plotted in Fig. 21.

The actual measured pressures agreed quite closely with the theoretical values for altitudes up to 120,000 feet, at which point the measured values became appreciably higher than the theoretical ones. The pressure range of the gauge in flight has a fundamental limitation in that the output pulse count decreases with pressure until a point is reached where the measuring interval becomes so long that the rate of change of pressure must be considered. In the Nike-Cajun flights this occurs at a pressure of approximately 0.5 mm Hg, where the gauge output is one pulse per second and the change of pressure due to vehicle motion is approximately 20 percent of the value being measured. This level is identified in Fig. 25 as the minimum pressure gauge reading for good resolution. This is seen to be

---

* See Appendix A for derivation.

† $\gamma = 1.4$ for air up to approximately 300,000 feet where the composition of the air begins to change.

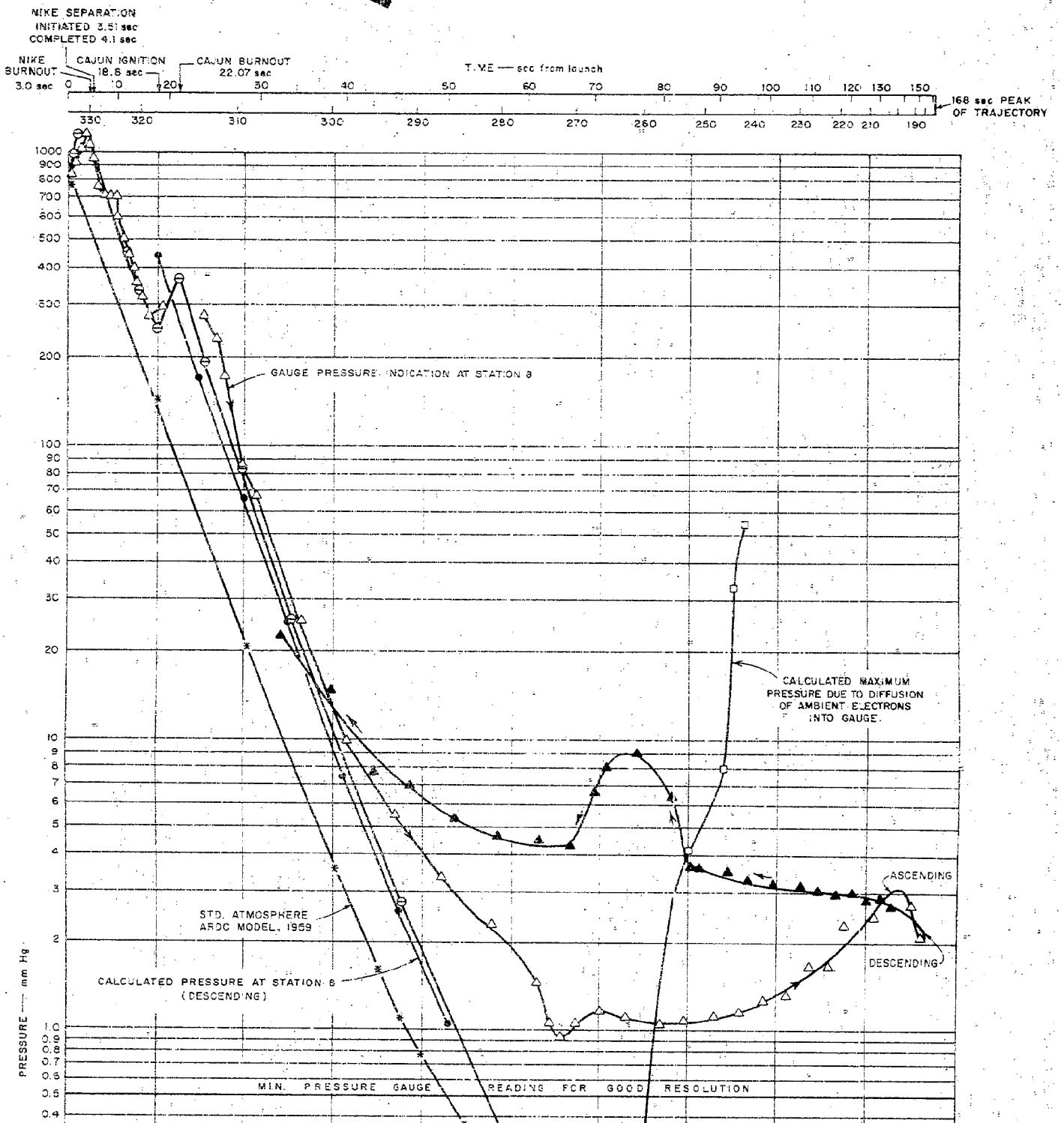
NIKE SEPARATION
INITIATED 3.51 sec
COMPLETED 4.1 sec
NIKE BURNOUT 3.0 sec
CAJUN IGNITION 18.6 sec
CAJUN BURNOUT 22.07 sec
TIME — sec from launch
168 sec PEAK OF TRAJECTORY
GAUGE PRESSURE INDICATION AT STATION 8
CALCULATED MAXIMUM PRESSURE DUE TO DIFFUSION OF AMBIENT ELECTRONS INTO GAUGE.
ASCENDING
DESCENDING
STD. ATMOSPHERE ARDC MODEL, 1959
CALCULATED PRESSURE AT STATION 8 (DESCENDING)
MIN. PRESSURE GAUGE READING FOR GOOD RESOLUTION
PRESSURE — mm Hg

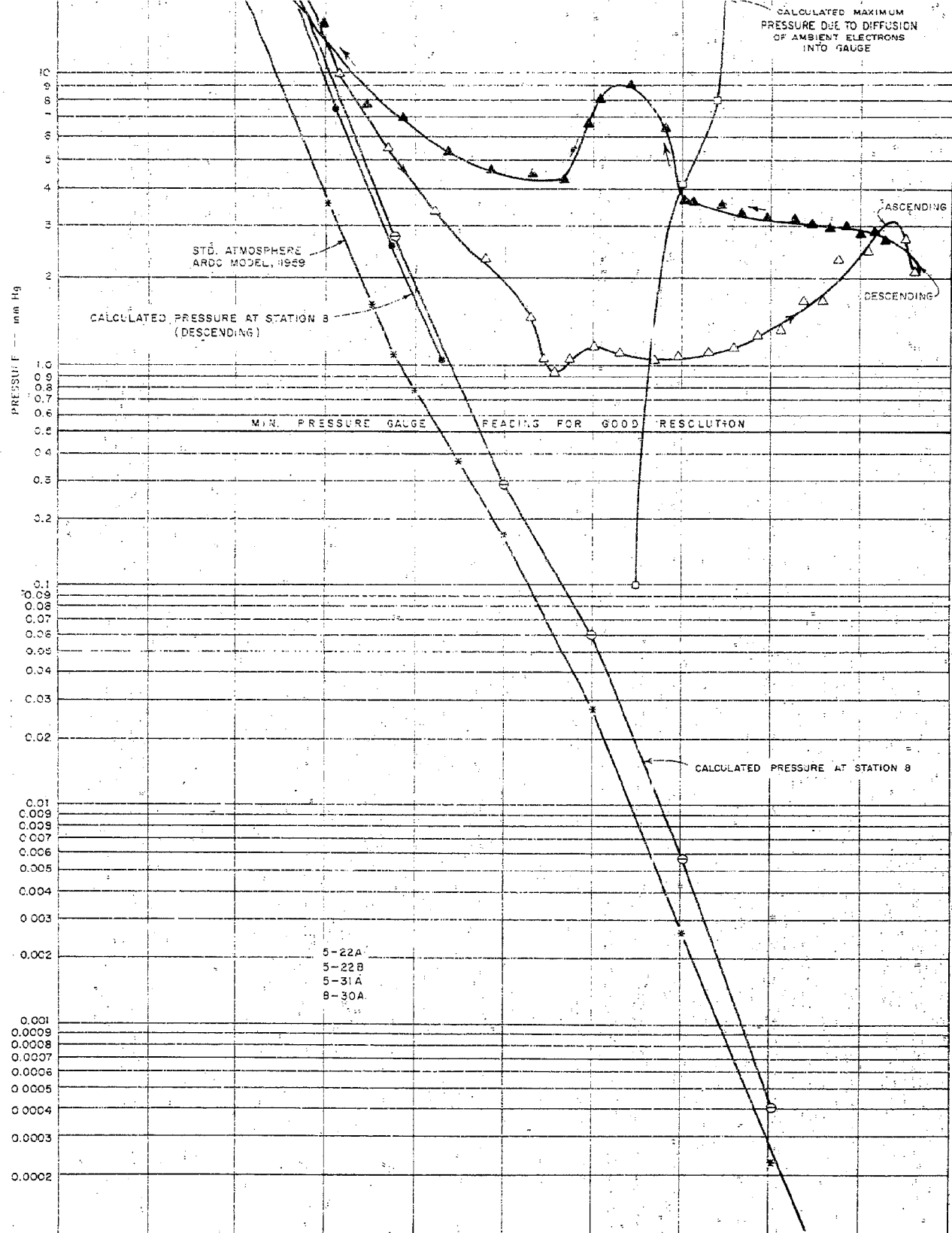
CALCULATED MAXIMUM
PRESSURE DUE TO DIFFUSION
OF AMBIENT ELECTRONS
INTO GAUGE
ASCENDING
DESCENDING
STD. ATMOSPHERE
ARDC MODEL, 1959
CALCULATED PRESSURE AT STATION 8
(DESCENDING)
MIN. PRESSURE GAUGE READING FOR GOOD RESOLUTION
CALCULATED PRESSURE AT STATION 8
5-22A
5-22B
5-31A
8-30A
PRESSURE — mm Hg
10
9
8
7
6
5
4
3
2
1.0
0.9
0.8
0.7
0.6
0.5
0.4
0.3
0.2
0.1
0.09
0.08
0.07
0.06
0.05
0.04
0.03
0.02
0.01
0.009
0.008
0.007
0.006
0.005
0.004
0.003
0.002
0.001
0.0009
0.0008
0.0007
0.0006
0.0005
0.0004
0.0003
0.0002

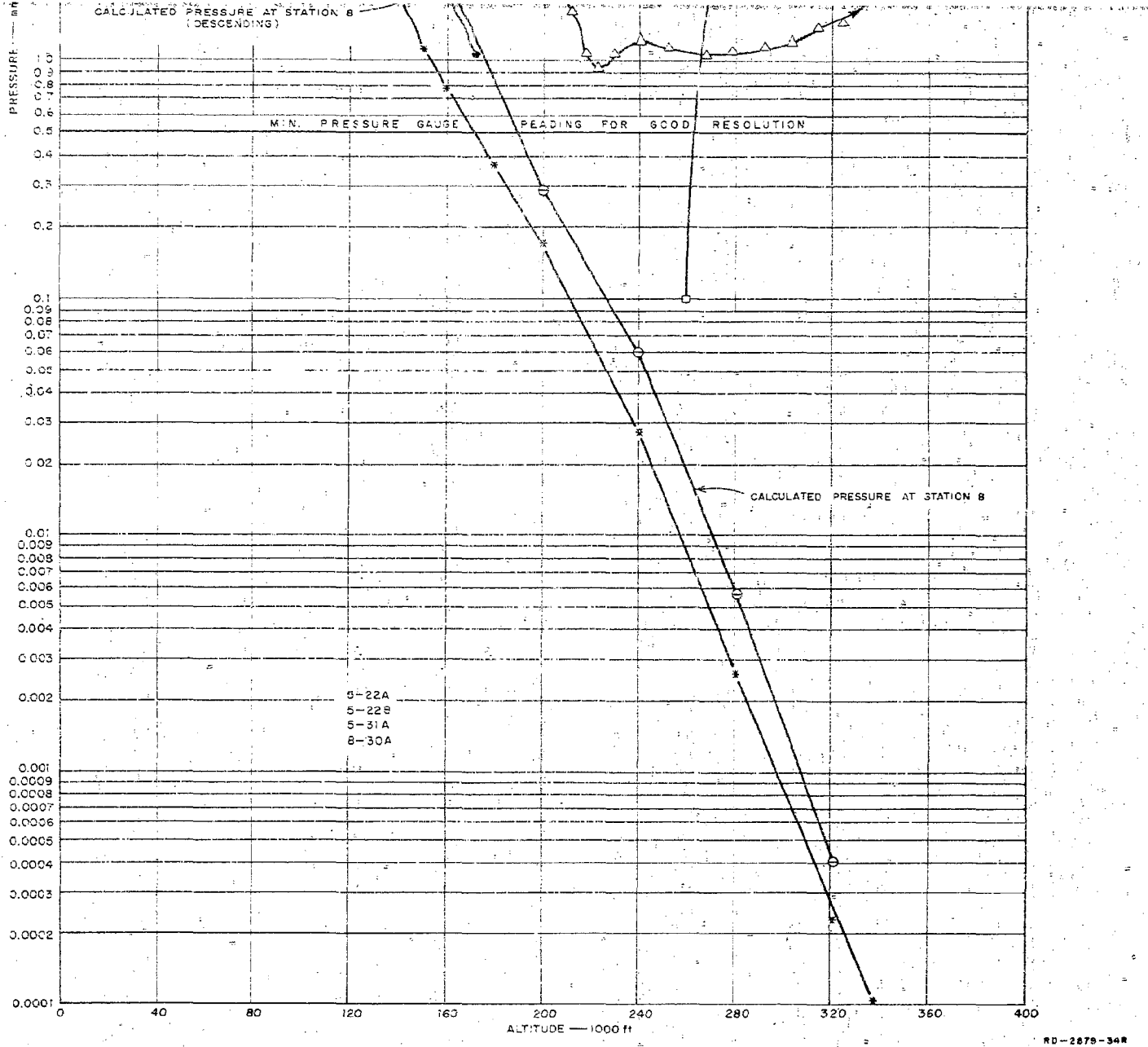

FIG. 25 FREE-STREAM PRESSURE, AND SURFACE PRESSURE AT STATION 8 vs. ALTITUDE AND TIME – ROCKET AA6.801

considerably lower than the pressure at which deviation of the theoretical and measured curves take place. Consequently, the observed discrepancies above 120,000 feet are not attributed to this effect.

Another possibility considered was that the ambient electron density was high enough to cause erroneous indications in the ionization gauge. The characteristic time constant of the pickup tube and chamber system was found to be less than 10 ms, a value low enough to assure essentially equal pressures inside and outside due to the relatively slow time rate of pressure change on the outside. Therefore, since there is negligible net gas flow through the tube in which to transport electrons, a diffusion current appears to be the only manner of contributing electrons to the densitometer from external sources. It was calculated that the mean free path is large enough at 270,000 ft so that free molecular flow rather than viscous flow exists in the pickup tube. At altitudes below 180,000 ft, the opposite is true. A transition region exists in the 180,000- to 270,000-ft region. The electron current due to diffusion has a maximum value at 180,000 feet equal to:

$$I \ \frac{\text{electrons}}{\text{sec}} \ \approx \ 100 \times n_e \ \frac{\text{electrons}}{\text{cc}} \qquad (7)$$

where

n_e = ambient electron density.

In the free-molecular flow region the expression for maximum I is

$$I \ \frac{\text{electrons}}{\text{sec}} \ \approx \ 2 \times 10^3 \times n_e^2 \ . \qquad (8)$$

The current I was calculated as a function of altitude, using Eqs. (7) and (8), for the appropriate altitude regions.* The current I in the intermediate region was obtained by interpolation, assuming a continuous transition. These currents were then used to calculate an equivalent gauge output by means of the following equation:

$$\text{pulse rate} \ = \ I \ (\text{amperes}) \times (5 \times 10^{10}) \ .$$

* Calculated values of electron current assume the worst case and neglect the loss of electrons to the walls of the tube connecting the gauge to missile surface.

Equivalent pressure readings were obtained from the manufacturer's calibration sheets, using the calculated values of pulse rate. These equivalent pressure readings, which are plotted in Fig. 25, indicate that ambient electron densities did not contribute significantly to the gauge errors noted above 120,000 feet, since the graph shows no appreciable ambient effects occurring before 250,000 feet. The graph also shows that the ambient effects which occur beyond 240,000 feet do not resemble the observed errors. It is nevertheless felt that an electron current into the gauge is a likely cause of false high readings at low pressures and that while currents produced by external ionization do not appear to be the only cause, they undoubtedly contributed to the observed error. However, the mechanism by which spurious electron current of proper magnitude could have entered to produce the observed errors remains unknown.

The pressure at Station 42.5 (location of center of VHF antenna) was not measured, since this location is five diameters back on the cylindrical portion of the rocket, where ambient pressure conditions exist.

4. Power Supply Voltages

In-flight measurements of the 28-volt, 6-volt, 150-volt and 1-cps supplies show no large deviations. This indicates that the *X*-band failure at launch occurred within the transmitter. Graphs of these voltages are given in Fig. 26.

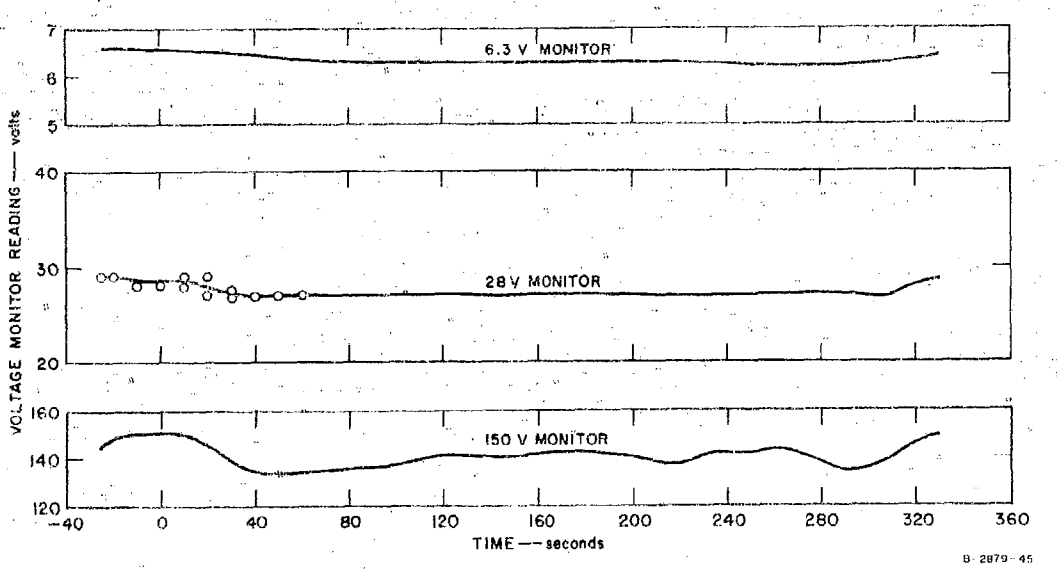

FIG. 26 EQUIPMENT MONITOR VOLTAGES vs. TIME – ROCKET AA6.801

5. VHF Antenna Breakdown Data

These data were derived mainly from the records of signal strength obtained at the A-6 and B-3 telemetry stations. Figure 27 shows breakdown initiate and extinguish values expressed in terms of percent of maximum transmitted power. The data points were obtained by examining the modulation waveform of received signal strength and noting the exact times in the cycle at which breakdown was initiated and extinguished. Since the power variation was approximately linear, the ratio of initiate or extinguish power to the maximum power was readily determined. (See Section II-B.)

It was found that the waveform of incident power as obtained from the telemetered detector data was very similar to the waveform of VHF signal strength. In Fig. 28, these waveforms are compared for a typical one-second interval at t = 45 seconds from launch. The curve of incident power has a shape almost identical to the curve of transmitted power, rather than the shape expected. Figure 28(b) compares the incident and transmitted power with respect to the level at which the characteristic step occurs, as a function of altitude. These curves are also almost identical. This suggests that the apparent breakdown took place in the transmission system ahead of the directional coupler. However, it is also possible that the incident power varied due to reflections from the aperture if breakdown was taking place there. Slight differences were noted between the data for the ascending phase and the data for the descending phase. Since breakdown is a function of density, some differences would be expected, as the density conditions across the gap are not the same for ascending and descending. This is attributable to the fact that even though the pressure conditions are approximately the same at a given altitude, the temperatures at the surface (Fig. 24), and hence in the boundary layer are quite different, resulting in a different value of density.

The initiate levels are replotted in Fig. 29, together with the results previously obtained in laboratory tests. The latter results indicate that at altitudes up to about 180,000 feet, less power is required to initiate breakdown as the density is decreased, whereas above 180,000 feet more power is required as the density is decreased.

In view of this, and the fact that the density was higher in the descending phase than in the ascending phase at all altitudes above 40,000 feet, one would expect lower initiate levels in the descending phase above

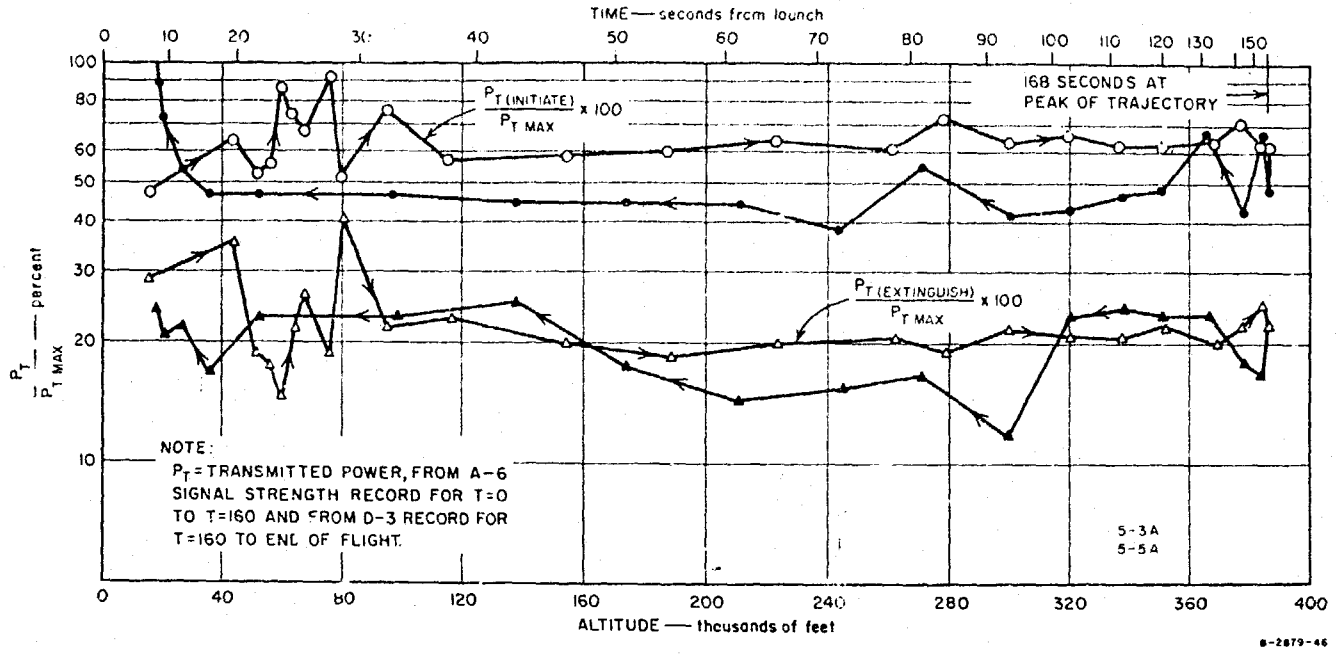

FIG. 27 ANTENNA BREAKDOWN INITIATE AND EXTINGUISH LEVELS vs. ALTITUDE AND TIME – ROCKET AA6.801

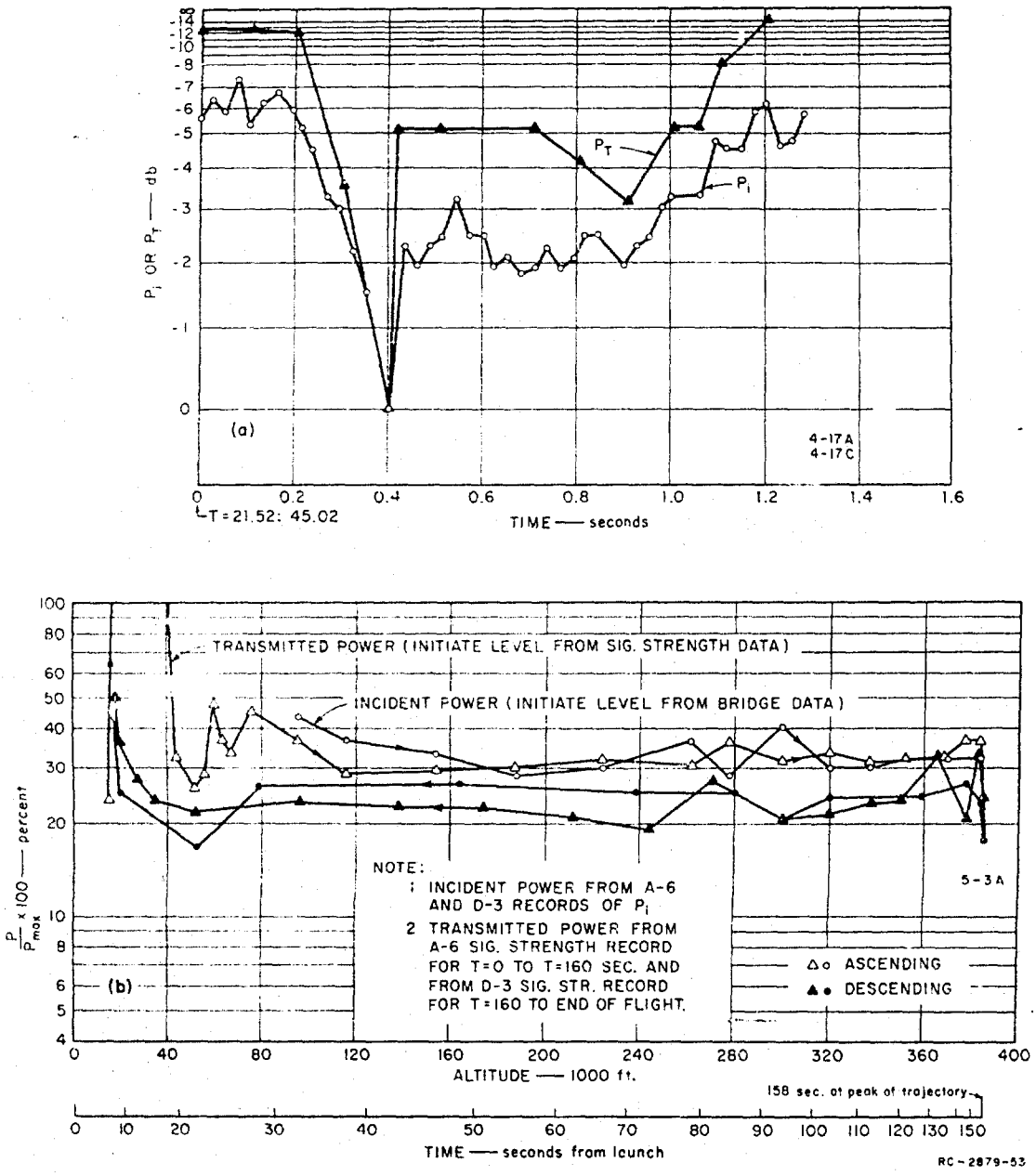

FIG. 28 COMPARISON OF BREAKDOWN INITIATE POWER DATA OBTAINED FROM VHF SIGNAL STRENGTH AND TELEMETRY RECORDS

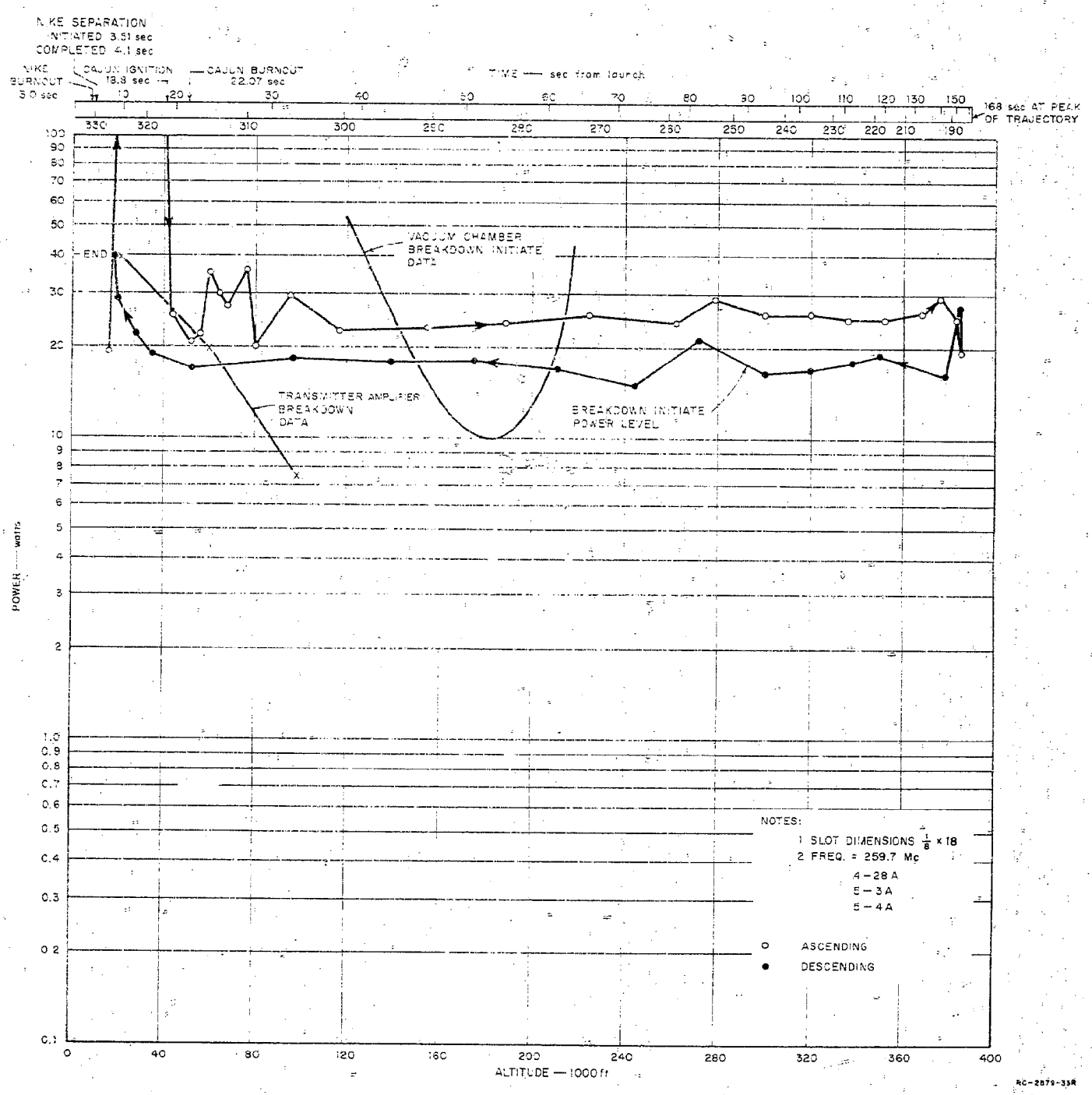

FIG. 29 ANTENNA BREAKDOWN INITIATE LEVELS

180,000 feet and higher levels below. This was not the case, however; Figs. 27, 28, and 29 show that lower values of initiate level were required in the descending phase below 180,000 feet.

A more fundamental discrepancy is obvious from Fig. 29. Whereas theory and laboratory experiments predict a breakdown altitude region of 120-240,000 feet, with a definite minimum value of initiate power at 180,000 feet, the flight data show a leveling-off to a more or less constant value at all altitudes above 120,000 feet. The available data indicate that the density conditions at a given altitude or pressure were only slightly different in the flight condition from what they were in the laboratory. Consequently, the large differences indicated in Fig. 29 are not explained in terms of known density differences.

The fact that breakdown occurred at lower altitudes than expected might be attributed to breakdown within the VHF amplifiers feeding the antenna. Two amplifiers in series composed the output stages of each VHF transmitter. Originally, RF breakdown in either amplifier stage was not considered a possibility by the subcontractor who assembled the VHF transmitters. However, the subcontractor later informed the Institute that the final stage might be expected to undergo breakdown at some altitudes. Consequently the final amplifier in the second and third flight packages, which were then being readied for flight, were carefully sealed at the launch site. Although it was not possible to check the seal in a vacuum chamber, it is presumed that the seal was complete.

Test data obtained later from the amplifier manufacturer show that at a power level of 40 watts, RF breakdown has occurred in at least two unpressurized amplifiers at a pressure equivalent to 20,000 feet altitude. Similarly, at power levels of 20 watts and 7.5 watts, breakdown has occurred in samples at altitudes of 60,000 and 97,000 feet, respectively. These data points are shown in Fig. 29. Since the first amplifier in each flight package was not sealed and since its output at the peak of the modulation cycle was 7.5 watts, breakdown could have occurred in it, on the basis of the above laboratory data. However, the flight data indicate that the breakdown level of output power of the final amplifier was approximately 20 watts at 97,000 feet, which corresponds to 3.17 watts output of the first amplifier. The latter value is considerably lower than that which was obtained in the lab. Because of the lack of complete data it is not certain that the breakdown actually took place in the transmitter amplifiers.

6. *X*-Band Antenna Breakdown Data

No *X*-band breakdown data were obtained. Figure 30 shows the expected results. The laboratory data of Fig. 15, which were plotted as a function of pressure, have been replotted in Fig. 30 as a function of altitude, with allowance for the dynamic conditions of temperature and pressure which existed at the aperture of the antenna during the flight. Separate curves are drawn for the ascending and descending phases, since pressure and temperature conditions are somewhat different (see also Figs. 24 and 25).

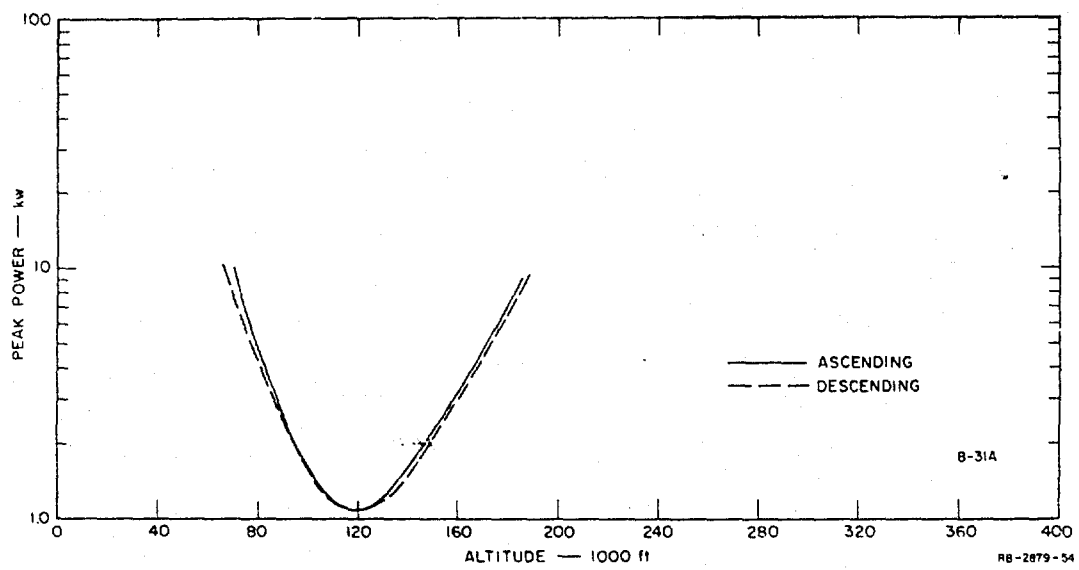

FIG. 30 X-BAND ANTENNA BREAKDOWN – CALCULATED FLIGHT DATA

7. VLF Data[5]

The VLF receivers recorded only the signal strength of U.S. Naval Radio Station NBA because a change in frequency of station NSS was made shortly before the last two flights. An excessive amount of antenna noise was noted throughout the entire flight, and is attributed to interference from the *S*-band beacon transmitter.

Accurate signal strength data were derived from the recorded receiver voltages, except at altitudes above 180,000 feet, where the rocket tumbled or precessed. The details of this motion are not known because the attitude-sensing magnetometer failed to operate above 135,000 feet. Consequently, signal strength data which was obtained for this higher altitude region contains a possible error of as much as 10 db.

Antenna impedance data were obtained as a function of altitude. The measured capacity of 30.1 picofarads (pf) just prior to Nike separation compared well with the 33 pf previously obtained from model measurements. Similarly the capacity after separation was 26.5 pf, as compared with 25.5 pf on model measurements. Between 9,000 and 210,000 feet a noise-like variation of about 7 pf (peak-to-peak) was noted. The reason for this is unknown but it is believed to be partly due to changes in the capacity of the dielectric gap.

Measured differences of about 4 pf were observed between the up and down paths at 30,000 feet, with smaller differences at the higher altitudes. These also are attributed to slight changes in the gap capacity.

At altitudes above 210,000 feet, as the rocket entered the ionosphere, the main trend was toward increasing capacity with increasing ionization with values rising to as high as four times the initial value near the peak of the trajectory. Superimposed on this are cyclic variations which are attributed to rocket precession. The reason for the main trend was not determined.

The conductance component showed a rise and fall in the 45,000 to 150,000 feet altitude region which has been attributed to heating of the gap by heat conduction from the Cajun motor, followed by cooling after burnout. A rise occurred on the down path at about 60,000 feet, probably as a result of aerodynamic heating.

8 Static Field Strength Data

The field meter experiment was directed at the investigation of possible effects of rocket engines in producing static charges on rockets and missiles. Previous experience with jet engine charging on aircraft indicated that the rocket engines should be expected to charge the vehicle to potentials of several thousand volts. Conductivity data indicated that this charge should leak away rapidly after burnout, so that it was anticipated that at altitudes of 30 kilometers and above the insensitive field meter used in this experiment should indicate zero.

Data from the firing shown in Fig. 31 indicate that the engines did indeed charge the rocket to potentials of several thousand volts, and, as was expected, this charge leaked away within a few seconds. Thus, shortly after burnout, the field meter indicated essentially zero field until an

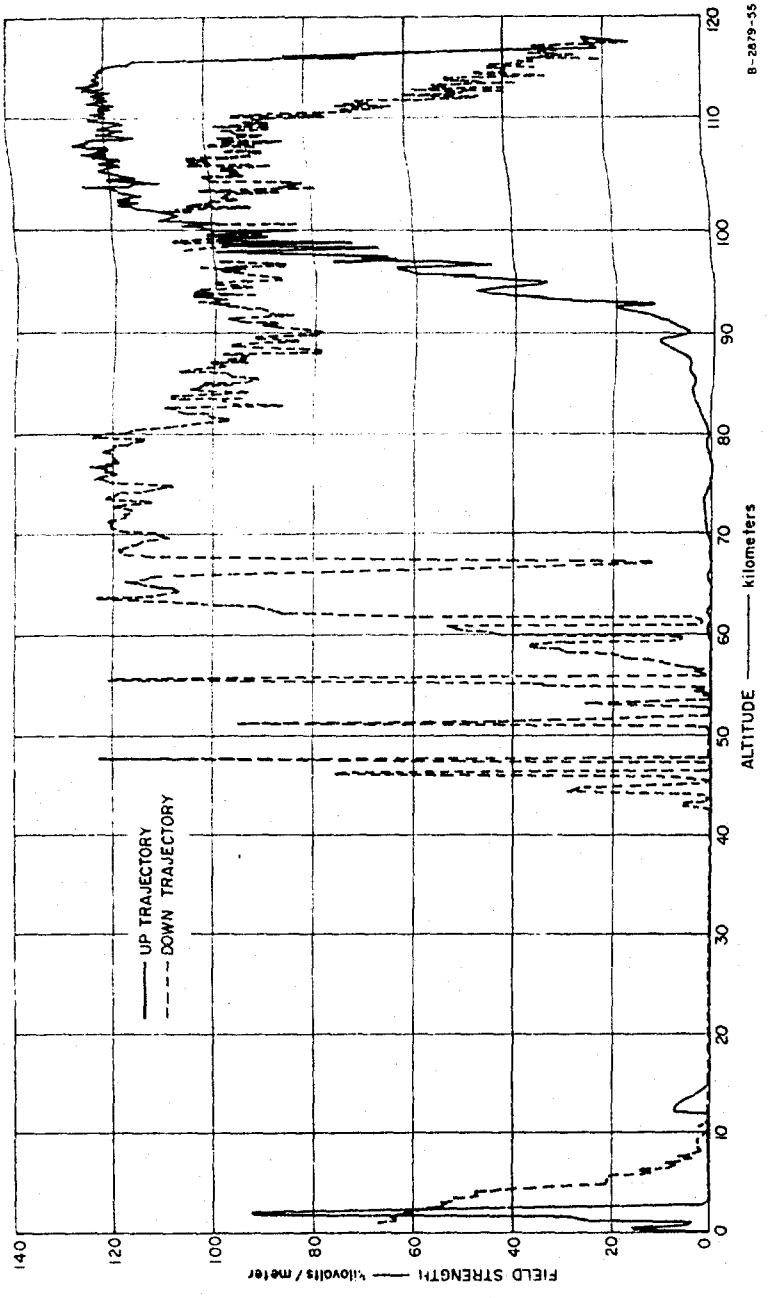

FIG. 31 MAGNITUDE OF ELECTROSTATIC FIELD vs. ALTITUDE

altitude of 90 km was reached. At this time the field meter unexpectedly began to indicate a non-zero field. The indicated field intensity gradually increased until at 100 km it reached a value of thousands of volts per meter. High field readings of gradually varying magnitude persisted to the apex of the trajectory and down to roughly 65 km.

When the data were first inspected it was felt that the high indicated field at 90 km and beyond must be the result of a malfunction in the field meter. It was difficult, however, to conceive of a malfunction that would cause the indicated field to vary gradually. On the other hand, assuming that the instrumentation did not malfunction, it was difficult to conceive of a mechanism whereby sufficient charge could be maintained on the rocket to produce the measured field magnitudes or ion currents. One possibility considered thus far is that the rocket encountered a cloud of dust near the apex of its trajectory, and triboelectric charging resulting from impacts with dust particles was responsible for the high charge on the rocket. The existence of a dust cloud at these altitudes was demonstrated by Soberman[9] of AFCRL using an Aerobee-Hi rocket equipped with traps to obtain dust samples. Unfortunately, Soberman's experiment did not measure the charges generated by the particles upon impact with the vehicle so that it is not possible to obtain quantitative verification of the indicated field magnitudes.

D. THIRD FLIGHT--ROCKET AA6.802

Rocket AA6.802 was launched from Eglin Gulf Test Range on 24 March 1961. Radar and camera records show that the rocket performed as expected. No data were obtained due to a failure of the power supply during the first acceleration shock of Nike ignition. No telemetry data were available to enable determination of the location of the failure. Data up to the instant of firing indicate that all systems were operating normally until that time.

IV CONCLUSIONS AND RECOMMENDATIONS

Although three payloads were launched and the rockets performed as expected, significant results were obtained only from the 14 March mission. Failures occurred in the common power supplies in the 4 November and 24 March payloads, thereby preventing the recording of useful data.

Data from the 14 March mission were limited because of a failure in the *X*-band transmitter shortly after launch and breakdown in the VHF system ahead of the antenna. Temperature profiles and nosecone pressure were obtained, as well as static charge and VLF field strength data.

In order for the primary objective, as set forth in the introduction, to be achieved, additional tests would be required. A fundamental difference exists between flight and wind tunnel conditions which would make the results of wind tunnel testing of questionable value. The free-stream velocity and pressure can be readily simulated, and perhaps even the density, but the free-stream and stagnation temperatures would in general not be the same in the wind tunnel as they are in flight, resulting in a different density profile across the boundary layer. Since this layer is where the breakdown occurs, and since breakdown is a function of density, different results would be obtained. In view of this, it is recommended that further tests should be flight tests. The usefulness of such tests would be increased if performed at speeds above Mach 6, where velocity and ionization effects would be readily apparent.

Two methods of increasing the reliability of such tests are suggested. First, because of the equipment failures experienced in the three flights it is recommended that at least one complete equipment package be available solely for environmental testing to destruction. The shock and vibration testing performed in this program was limited because the equipment tested was flight equipment and could not be tested beyond its endurance.

Second, it is felt that the use of separate power supplies for each experiment and for the telemetry equipment would be the proper approach for flight tests, notwithstanding the fact that a larger vehicle would be required. This approach was not used in the program described here because

of severe space limitations in the Nike-Cajun instrumentation package. An alternative would be to use the same vehicle (Nike-Cajun) with only one major experiment (*i.e.* cw or pulse breakdown) per flight. In this case, a minimum of two flights would be required. Additional reliability could then be readily achieved by decreasing the density of all critical equipment and utilizing the remaining space for detectors enlarged by the addition of integral amplifiers to eliminate low-level signals, which are susceptible to stray pickup. The elimination of inter-experiment interference problems and a reduction in ground instrumentation complexity would also result from this approach. Another alternative would be to utilize extra space on another vehicle on a non-interfering basis.

APPENDIX

PRESSURE ON SURFACE OF CONE AS A FUNCTION OF FREE-STREAM PRESSURE AND MACH NUMBER

APPENDIX

PRESSURE ON SURFACE OF CONE AS A FUNCTION OF FREE-STREAM PRESSURE AND MACH NUMBER

The normalized pressure change between the free stream and the surface of a cone for a given Mach number and cone semi-vertex angle has been determined by Taylor and Maccoll[10] and is given by

$$\frac{\Delta P}{q} = \frac{P_2 - P_1}{q} \tag{A-1}$$

where P_2 = cone surface pressure, P_1 = free-stream pressure, and q is a reference pressure given by

$$q = \frac{\rho V^2}{2} = \frac{\rho (aM)^2}{2} \tag{A-2}$$

ρ = density
V = velocity of body
a = local speed of sound
M = Mach number.

But

$$a^2 = \frac{\gamma P}{\rho}$$

γ = ratio of specific heats (1.4 for air)
P = pressure of gas

so that

$$q = \frac{\gamma}{2} PM^2 \tag{A-3}$$

Equation (A-1) then becomes

$$P_2 - P_1 = \frac{\gamma}{2} P_1 M_1^2 \frac{\Delta P}{q} .$$

or

$$P_2 = P_1 + \frac{\gamma}{2} P_1 M_1^2 \frac{\Delta P}{q}$$

$$P_2 = P_1 \left(1 + \frac{\gamma}{2} M_1^2 \frac{\Delta P}{q}\right) . \qquad \text{(A-4)}$$

PRINCIPAL PROJECT PERSONNEL

1. T. Morita—Head, Radiation Systems Group
2. Chown, John B.—Senior Research Engineer and Project Leader
3. Keenan, Michael G.—Research Engineer
4. Spitzer, Ewald E.—Mechanical Engineer
5. Wadsworth, Willard C.—Engineering Assistant

ACKNOWLEDGMENT

The authors thank Mr. Charles Ellis of AFCRL for his invaluable assistance in the necessary planning and liaison connected with all phases of the work and for the many long hours of tireless effort he contributed during the pre-launch preparation of the instrument packages at the Eglin Gulf Test Range.

Special thanks go to Mr. William K. Vickery of APGC, Eglin AFB, who was extremely helpful in scheduling and directing the missile launchings and mission support functions. The authors are indebted to Mr. Claud Gwinn, Mr. Don Lynch and Mr. Dahl Mitchell of the University of Oklahoma Research Foundation for their assistance in the check-out of the telemetry equipment and the recording of the telemetry data during the flights.

The authors acknowledge the cooperation and valuable assistance of Mr. John B. Lomax of SRI for his countless contributions to the project.

REFERENCES

1. J. Gould and L. W. Robert, "Breakdown of Air at Microwave Frequencies," *J. Appl. Phys.* 27, *10*, pp. 1162-1170 (October 1956).

2. A. D. MacDonald, "High Frequency Breakdown of Air at High Altitudes," *Proc. IRE* 47, *3*, p. 436 (March 1959).

3. S. C. Brown, "High Frequency Gas Discharge Breakdown," *Proc. IRE* 39, *12*, pp. 1493-1501 (December 1951).

4. J. B. Chown, "Study of Plasma-Induced Voltage Breakdown at Low Pressure," Final Report, SRI Report 3369, Contract AF 33(600)-41517, Stanford Research Institute, Menlo Park, California (July 1961).

5. J. B. Lomax, "Measurements of VLF Transmission Characteristics of the Ionosphere with Instrumented Nike-Cajun Rockets," Final Report, SRI Project 3274, Contract NOw60-0405(FBM), Stanford Research Institute, Menlo Park, California.

6. W. K. Vickery, "Nike-Cajun Vertical Probe Firing Report," APGC-TN-61-21, Eglin Air Force Base, Florida (May 1961).

7. R. A. Minzner, K. S. W. Champion, and H. L. Pond, "The ARDC Model Atmosphere, 1959," AFCRC-TR-59-267 (August 1959).

8. E. A. Bonney, *Engineering Supersonic Aerodynamics*, pp. 179-180 (McGraw-Hill Book Company, Inc., New York City, 1950).

9. *Newsweek*, p. 63 (July 3, 1961).

10. E. A. Bonney, *op. cit.*, p. 180.

The following material, although not explicitly referred to in the text, is also pertinent.

1. J. Chown, W. Scharfman, and T. Morita, "Voltage Breakdown Characteristics of Microwave Antennas," *Proc. IRE* 47, 8 (August 1959).

2. Saul Dushman, *Vacuum Technique* (John Wiley and Sons, New York City, 1949).

3. A. G. Hammitt, and K. R. A. Murthy, "Approximate Solutions for Supersonic Flow over Wedges and Cones," Report 449, Contract AF 49(638)-465, Princeton University, Princeton, N. J. (April 1959).

4. Edward C. Jordan, *Electromagnetic Waves and Radiating Systems* (Prentice, Hall, Inc., New York City, 1950).

5. W. E. Scharfman, and T. Morita, "Voltage Breakdown of Antennas at High Altitudes," Technical Report 69, SRI Project 2494, Contract AF 19(604)-3458, Stanford Research Institute, Menlo Park, California (June 1958).

STANFORD RESEARCH INSTITUTE | MENLO PARK, CALIFORNIA

Regional Offices and Laboratories

SOUTHERN CALIFORNIA LABORATORIES
820 Mission Street
South Pasadena, California

WASHINGTON OFFICE
808 17th Street, N.W.
Washington 5, D.C.

NEW YORK OFFICE
270 Park Avenue, Room 1770
New York 17, New York

DETROIT OFFICE
The Stevens Building
1025 East Maple Road
Birmingham, Michigan

EUROPEAN OFFICE
Pelikanstrasse 37
Zurich 1, Switzerland

Representatives

HONOLULU, HAWAII
Finance Factors Building
195 South King Street
Honolulu, Hawaii

LONDON, ONTARIO, CANADA
85 Wychwood Park
London, Ontario, Canada

LONDON, ENGLAND
15 Abbotsbury Close
London W. 14, England

MILAN, ITALY
Via Macedonio Melloni 40
Milano, Italy